Universidade do Minho
Escola de Engenharia

Yousaf Haroon

Mechanical characterization and concrete bond performance of GFRP rebars with graphene-modified epoxy matrix: comparison with conventional epoxy systems

FRP++
Advanced structural analysis and design using composite materials

Funded by the European Union

September 2026

Mechanical characterization and concrete bond performance of GFRP rebars with graphene-modified epoxy matrix: comparison with conventional epoxy systems

Yousaf Haroon

FRP++
Advanced structural analysis and design using composite materials

UMinho | 2026

The European Master in Advanced Structural Analysis and Design using Composite Materials is a join initiative of:

Universidade do Minho · Universitat de Girona · Università degli Studi di Napoli Federico II · INSA Institut National des Sciences Appliquées Toulouse · Université de Toulouse

Universidade do Minho
Escola de Engenharia

Yousaf Haroon

Mechanical characterization and concrete bond performance of GFRP rebars with graphene-modified epoxy matrix: comparison with conventional epoxy systems

FRP++
Advanced structural analysis and design using composite materials

Master Dissertation
European Master Advanced Structural Analysis and Design using Composite Materials

Work developed under the supervision of
Doctor Luís Luciano Gouveia Correia
Eng. Nuno Fraga Roque

Funded by
the European Union

September 2026

DIREITOS DE AUTOR E CONDIÇÕES DE UTILIZAÇÃO DO TRABALHO POR TERCEIROS

Este é um trabalho académico que pode ser utilizado por terceiros desde que respeitadas as regras e boas práticas internacionalmente aceites, no que concerne aos direitos de autor e direitos conexos.

Assim, o presente trabalho pode ser utilizado nos termos previstos na licença abaixo indicada.

Caso o utilizador necessite de permissão para poder fazer um uso do trabalho em condições não previstas no licenciamento indicado, deverá contactar o autor, através do RepositóriUM da Universidade do Minho.

Licença concedida aos utilizadores deste trabalho

[If the supervisor/author wishes to use one of the Creative Commons licences, they should choose and keep only one of the following icons and the corresponding lettering and URL, deleting the italicised text that follows. However, it is possible to choose another type of licence; in that case, the necessary information should be included by duly adapting this template.]



Atribuição CC BY

https://creativecommons.org/licenses/by/4.0/

[This licence allows others to distribute, remix, adapt, and build upon your work, even for commercial purposes, provided that they give you appropriate credit for the original creation. It is the most flexible of all available licences. It is recommended for maximising the dissemination and use of licensed materials.]

ACKNOWLEDGEMENTS

I would like to express my gratitude to my advisor, Dr. Luís Luciano Gouveia Correia, for his valuable advice, constant support, and constructive criticism in the course of preparing this dissertation. His professional advice, encouragement, and stimulating discussions have been essential in achieving the successful completion of this research work.

I would also like to thank my co-advisor, Engr. Nuno Fraga Roque from GRUN Portugal, for his technical advice and timely provision of material. His help and readiness to share his knowledge have positively influenced the quality of this research.

I would also like to express my thanks to the academic and technical staff of the University of Minho for their support, as well as for providing necessary facilities for conducting experiments. I am thankful to my friend Manzoor (PhD student UMinho), Mr. Matos and Ricardo (LEST Technicians) and Eng. Marco (LEST director) for their help during experiments.

I would also like to thank my family for their unconditional love and support in all my endeavors.

Finally, I gratefully acknowledge the financial support provided by the European Union for participation in the Erasmus Mundus FRP++ European Master Course in Advanced Structural Analysis and Design using Composite Materials (Project no. 101048961). This work was also supported by FCT/MCTES under the R&D Unit Institute for Sustainability and Innovation in Structural Engineering (ISISE), under the references UID/4029/2025 (DOI: 10.54499/UID/04029/2025), UID/PRR/04029/2025 (DOI: 10.54499/UID/PRR/04029/2025) and UID/PRR2/04029/2025 (DOI: 10.54499/UID/PRR2/04029/2025), and under the Associate Laboratory Advanced Production and Intelligent Systems (ARISE) under reference LA/P/0112/2020 (DOI: 10.54499/LA/P/0112/2020).

STATEMENT OF INTEGRITY

I hereby declare having conducted this academic work with integrity. I confirm that I have not used plagiarism or any form of undue use of information or falsification of results along the process leading to its elaboration.

I further declare that I have fully acknowledged the Code of Ethics and Conduct of the University of Minho.

DECLARATION ON THE USE OF ARTIFICIAL INTELLIGENCE (AI) TOOLS

I hereby declare having acted this academic work with integrity and confirm that I have not resorted to any form of undue use of AI tools, nor to the falsification or omission of information, sources, data, results or processes in any of the stages leading to its elaboration.

I further declare that any use of AI tools was done in a transparent and responsible manner, being duly noted in the work, and that I critically verified the accuracy of the content produced with their support, assuming full responsibility for what I submit.

I further declare that I have fully acknowledged the Code of Ethics and Conduct of the University of Minho, as well as the applicable standards of academic integrity and data protection.

Caracterização mecânica e desempenho de aderência do betão em varões de reforço de GFRP com matriz epóxi modificada com grafeno: comparação com sistemas epóxi convencionais.

RESUMO

Os varões de polímero reforçado com fibras de vidro (GFRP) constituem uma alternativa ao aço em estruturas de betão armado, sobretudo pela sua resistência à corrosão. Neste trabalho avaliou-se a influência da modificação da matriz epóxi com grafeno no comportamento mecânico e na aderência ao betão de varões de GFRP produzidos pela empresa portuguesa GRUN. Foram realizados ensaios de tração e de resistência ao corte transversal (TSS) em varões com matriz epóxi convencional (CE) e modificada com grafeno (GE), bem como ensaios de arrancamento em varões de 12 mm, com comprimentos de aderência de 5Ø e 10Ø. Varões comerciais Schöck ComBAR foram utilizados como referência. A modificação com grafeno conduziu a reduções de cerca de 16% na resistência à tração e no módulo de elasticidade. No entanto, o efeito na TSS dependeu do diâmetro do varão, variando entre uma redução de 12,8% para Ø6 e um aumento de 30,6% para Ø12. O aumento do comprimento de aderência de 5Ø para 10Ø aumentou a força máxima de arrancamento, mas reduziu a tensão média de aderência, evidenciando a distribuição não uniforme das tensões de aderência ao longo do comprimento aderente. A modificação com grafeno não produziu uma melhoria consistente da resistência de aderência, embora tenha influenciado a resposta força–deslizamento e o comportamento pós-pico. A observação de danos nas nervuras confirmou a importância da interação mecânica entre os varões e o betão. Por fim, uma análise inversa foi utilizada para identificar os parâmetros da lei local tensão de aderência–deslizamento, verificando-se uma boa representação de algumas respostas experimentais, mas limitações na reprodução do comportamento pós-pico e residual.

PALAVRAS-CHAVE: Epóxi convencional (CE); Epóxi modificado com grafeno (GE); Polímero reforçado com fibra de vidro (GFRP); Caracterização mecânica; Propriedades de tração; Resistência ao cisalhamento transversal (TSS); Comportamento de adesão; Teste de arrancamento direto (DPT); Relação tensão-deslizamento da adesão; Lei de adesão local; Interface fibra-matriz.

Mechanical Characterization and Concrete Bond Performance of GFRP Rebars with Graphene-Modified Epoxy Matrix: Comparison with Conventional Epoxy Systems

ABSTRACT

Glass fiber-reinforced polymer (GFRP) rebars provide an alternative to steel reinforcement in reinforced concrete structures, mainly due to their corrosion resistance. This study evaluated the influence of graphene modification of the epoxy matrix on the mechanical behavior and concrete bond performance of GFRP rebars manufactured by the Portuguese company GRUN. Tensile and transverse shear strength (TSS) tests were performed on rebars with conventional epoxy (CE) and graphene-modified epoxy (GE) matrices, while pull-out tests were conducted on 12 mm diameter rebars with bonded lengths of 5Ø and 10Ø. Commercial Schöck ComBAR rebars were used as a benchmark. Graphene modification resulted in reductions of approximately 16% in tensile strength and elastic modulus. However, its effect on TSS depended on the rebar diameter, ranging from a 12.8% reduction for Ø6 rebars to a 30.6% increase for Ø12 rebars. Increasing the bonded length from 5Ø to 10Ø increased the maximum pull-out force but reduced the average bond stress, reflecting the non-uniform distribution of bond stresses along the bonded length. Graphene modification did not produce a consistent improvement in bond strength, although it influenced the force–slip response and post-peak behavior. Damage observed in the surface ribs confirmed the importance of mechanical interaction between the rebars and the surrounding concrete. Finally, an inverse analysis was used to identify the parameters of the local bond stress–slip law. The model reproduced some experimental responses satisfactorily, although limitations were observed in representing the post-peak and residual behavior.

KEYWORDS: Conventional Epoxy (CE); Graphene-modified Epoxy (GE); Glass Fiber Reinforced Polymer (GFRP); Mechanical characterization; Tensile properties; Transverse Shear Strength (TSS); Bond Behavior; Direct Pull-Out Test (DPT); Bond Stress–Slip Relationship; Local bond law; Fiber–Matrix Interface.

TABLE OF CONTENTS

Acknowledgements iii
Resumo V
Abstract VI
Table of Contents VII
List of Figures IX
List of Tables X
List of Abbreviations and Symbols XI
1. Introduction 1
1.1. Motivation 1
1.2. Objectives 2
1.3. Structure of the thesis 3
2. State of the art 5
2.1. Materials characterization 5
2.1.1. Tensile testing 5
2.1.2. Transverse Shear Strength (TSS) Testing 8
2.2. Concrete bond performance 10
2.2.1. Surface treatment / features: 11
2.2.2. Bar diameter: 12
2.2.3. Bond length: 13
2.2.4. Concrete compressive strength: 13
2.2.5. Concrete confinement: 13
2.2.6. Environment/Temperature: 14
2.2.7. Matrix modification: 15
3. Experimental campaign 19
3.1. Materials characterization 19
3.1.1. Tensile testing 19

3.1.2. Transverse Shear Strength (TSS) testing 21
3.2. Concrete bond performance 22
4. Results and Discussion 27
4.1. Materials characterization 27
4.1.1. Tensile testing 27
4.1.2. Transverse Shear Strength (TSS) test 30
4.1.3. Comparative analysis of mechanical performance 33
4.2. Concrete bond performance 34
4.2.1. The Effect of bonded length and epoxy modification 36
4.2.2. Force–slip response and bond mechanisms 37
4.2.3. Failure observations 38
4.2.4. Fracture energy 39
4.2.5. Comparison of CE and GE systems 39
5. Parametric study 41
5.1. Analytical method for bond test 41
5.1.1. Local bond stress–slip relationship 42
5.1.2. Inverse analysis procedure 42
5.1.3. Comparison between experimental and analytical responses 44
5.1.4. Schock reference bars 45
5.1.5. Conventional epoxy GFRP bars 45
5.1.6. Graphene-modified epoxy GFRP bars 45
6. Conclusion, future work and recommendations 51
6.1.1. Conclusion 51
6.1.2. Future work and recommendations 52
7. References 53

LIST OF FIGURES

Figure 1: Failure mode of a) GFRP and b) CFRP rebars [4] 6

Figure 2: (a). Transverse shear testing set-up (b). Failure mode of GFRP rebars [35] 9

Figure 3: Bond stress transfer mechanism between GFRP bar and concrete [3] 11

Figure 4: Different types of commercially available FRP rebars[49] 12

Figure 5: Mechanical testing schematics and photo of the test 20

Figure 6: Transverse shear strength test schematics and photo of the test 21

Figure 7: Preparation of direct pull-out specimens: (a) positioning of GFRP bars and PVC sleeves in the formwork; (b) fixation and sealing of the bars prior to casting; (c) concrete casting; (d) concrete compaction using an internal vibrator; (e) and (f) preparation of testing 24

Figure 8: Pull-out test setup a) Schematics and b) photo of the test 25

Figure 9: Tensile test experimental results 27

Figure 10: Tensile samples a) Before test b) After test 29

Figure 11: TSS test curve for a) 6 mm b) 8 mm and c) 12 mm diameter GFRP rebars 30

Figure 12: a) Prepared TSS samples before testing, b) and c) tested samples of conventional and graphene-modified epoxy respectively 33

Figure 13: Pull-out test results a) Pull-out force vs slip and b) Bond strength vs slip 35

Figure 14: Failure mode of direct pull-out test 38

Figure 15: Comparison of experimental and analytical results of direct pull-out test a) and b) S_5Ø, c) and d) CE_5Ø, e) and f) GE_5Ø, g) and h) CE_10Ø and i) GE_10Ø 47

LIST OF TABLES

Table 1: Summary table showing the effect of graphene on mechanical properties..... 8

Table 2: Effect of nanomaterials matrix modification on rebar-concrete bond performance 17

Table 3: Variables and scheme for mechanical testing..... 20

Table 4: Summary of variables for pull-out test..... 23

Table 5: Summary of the tensile test results..... 28

Table 6: Results summary of TSS test. 31

Table 7: Result summary of the direct pull-out test 36

Table 8: Local bond stress-slip parameters resulted from analysis of the direct pull-out tests. 48

List of Abbreviations and Symbols

Abbreviations

ACI	American Concrete Institute
AFRP	Aramid Fiber Reinforced Polymer
ASTM	American Society for Testing and Materials
CEN	European Committee for Standardization
CFRP	Carbon Fiber Reinforced Polymer
CNTs	Carbon Nanotubes
DPT	Direct Pull-out Test
FTIR	Fourier-Transform Infrared Spectroscopy
GFRP	Glass Fiber Reinforced Polymer
GNP	Graphene Nanoplatelets
GO	Graphene Oxide
GPL	Graphene Platelets
SEM	Scanning Electron Microscopy
TSS	Transverse Shear Strength
Wt%	weight percentage

Symbols

A_b	Cross-sectional area of GFRP bar
c	Concrete cover
d_b	Bar diameter
E_{cm}	Modulus of elasticity of concrete
E_f	Modulus of elasticity of GFRP bar
f_{ck}	Characteristic compressive strength of concrete
f_{cm}	Mean compressive strength of concrete
f_{ctm}	Mean axial tensile strength of concrete
$f_{ctm,sp}$	Mean splitting tensile strength of concrete

f_{fu}	Ultimate tensile strength of GFRP bar
f_{yk}	Characteristic yield strength of steel
F	Applied pullout force
F_{max}	Peak pullout force
F_R	Residual pullout force
G_f	Fracture energy
K	Initial stiffness
L_a	Anchorage length
L_b	Embedment length / Bond Length
L_c	Distance between loaded section and LVDT attachment point
s_f	Free-end slip
$s_{f,max}$	Free-end slip at peak load
s_l	Loaded-end slip
$s_{l,max}$	Loaded-end slip at peak load
t	Time
δ	Measured displacement / average LVDT reading
ε	Strain
σ	Stress
σ_f	Tensile stress in GFRP bar
τ	Local bond stress
τ_{avg}	Average bond stress
τ_{adh}	Adhesion bond stress
τ_{max}	Bond strength / maximum average bond stress
τ_n	Normalized bond strength
τ_U	Transverse shear strength

THIS PAGE WAS INTENTIONALLY LEFT BLANK

1. INTRODUCTION

The construction industry in Europe continuously seeks innovative materials that can improve the durability, service life, and sustainability of reinforced concrete structures. Conventional steel reinforcement has been widely used for decades due to its high strength and ductility; however, its susceptibility to corrosion in aggressive environments remains one of the major causes of structural degradation and high maintenance costs. Steel reinforcement corrosion can significantly reduce the service life of concrete structures, particularly in marine environments, bridges, parking structures, and wastewater treatment facilities. Consequently, there has been increasing interest in developing non-corrosive alternatives capable of overcoming these limitations [1-3]

In the range of possible options, glass fiber reinforced polymer (GFRP) bars have gained much popularity on account of their corrosion immunity, high strength-to-weight ratio, low density, and electromagnetic neutrality. However, although there are many advantages of GFRP bars, there are also several problems that hinder their structural use. Firstly, GFRP bars differ from steel reinforcement bars with regard to the mechanical characteristics owing to their anisotropic behavior and presence of a polymeric matrix. Secondly, stress transfer in GFRP bars is influenced by polymeric matrix, and is responsible for mechanical properties in the transversal direction as well as the bond behavior with surrounding concrete. [4-5]

The recent developments in the field of nanotechnology provide some possible ways of enhancing the performance of FRPs. The use of several nanomaterials is possible; however, among all, graphene stands out as the most promising due to its unique mechanical strength, large surface area, and high interface strengthening ability. The addition of graphene to epoxy resin could help in enhancing the fiber-matrix interface, providing improved crack resistance and increased matrix-dominated property strength, which could ultimately enhance the mechanical strength of GFRP bars and their performance in concrete.[1], [5-7]

1.1. Motivation

The growing demand for durable and maintenance-free reinforced concrete structures has accelerated the use of Fiber Reinforced Polymer (FRP) reinforcing bars as an alternative to conventional steel reinforcement. Although GFRP bars eliminate corrosion-related problems, their structural performance is still influenced by the properties of the polymer matrix, particularly with respect to transverse shear

resistance and bond behavior with concrete. Since effective load transfer between fibers, matrix, and surrounding concrete is essential for structural performance, improving the characteristics of the epoxy matrix remains an important research challenge.

Graphene has attracted significant research interest because of its ability to enhance the mechanical performance of polymer composites even at relatively low concentrations. Previous studies have reported improvements in epoxy-based composites through graphene incorporation; however, limited information is available regarding its influence on the combined tensile behavior, transverse shear strength, and concrete bond performance of GFRP reinforcing bars. Furthermore, the relationship between improvements in matrix-dominated properties and the resulting bond behavior has not yet been fully established.

Motivated by these research gaps, this study investigates whether modifying the epoxy matrix with graphene can improve both the intrinsic mechanical properties of GFRP reinforcing bars and their bond performance with concrete. The outcomes of this work aim to contribute to the development of more reliable and durable GFRP reinforcement for future civil engineering applications.

1.2. Objectives

The main objective of this research is to investigate and study the influence of graphene modification of the epoxy matrix on the mechanical properties and bond behavior of GFRP reinforcing bars through an experimental study. To achieve this objective, tensile tests were performed to evaluate the tensile strength, elastic modulus, ultimate tensile strain, and failure behavior of conventional epoxy and graphene-modified epoxy GFRP bars. In addition, transverse shear tests following ASTM D7617/D7617M were conducted to investigate the effect of graphene on the matrix-dominated shear properties of the reinforcement. Lastly, direct pull-out tests were performed using ASTM D7913/D7913M standard [8] to assess the bond performance between GFRP bars and concrete by evaluating the bond stress–slip behavior, ultimate bond strength, and failure mechanisms. Through these experimental investigations, the study aims to investigate the effectiveness of graphene-modified epoxy in enhancing the overall performance of GFRP reinforcing bars and to provide a better understanding of its potential application in reinforced concrete structures.

1.3. Structure of the thesis

Chapter 1 describes the background and motivation of the investigation, with special emphasis on the drawbacks and limitations of conventional GFRP rebars and the potential offered by epoxy resins reinforced with graphene. It also defines the research objectives, scope of the study, and the importance of the proposed research.

Chapter 2 gives a review of the existing state of the art with respect to GFRP rebars. Mechanical characterization of GFRP rebars, namely, their tensile strength, transverse shear strength, and bond behavior of GFRP reinforcement in concrete are discussed. Also included in this chapter is an overview of the effect of graphene and other nanomaterials on FRP composite properties.

Chapter 3 provides information on the sample preparation process and the experimental approach used in this research. It highlights the manufacturing process of traditional and graphene reinforced GFRP bars, as well as the concrete mixed design, and test methods conducted in accordance with the relevant ASTM standard.

Chapter 4 presents and critically discusses the experimental results obtained from the tensile, transverse shear, and direct pull-out tests. The influence of graphene modification, bar diameter, and bonded length on the mechanical and bond performance of the GFRP bars is evaluated and compared.

Chapter 5 demonstrates the analytical investigation of the local bond behavior using the inverse analysis approach. The experimental pull-out responses are compared with the analytical predictions, and the local bond-slip parameters and fitting accuracy are discussed for the different reinforcement configurations.

Chapter 6 summarizes the main findings of experimental and analytical investigations and highlights the key effects of graphene modification and bonded length. Recommendations for future research are also presented, focusing on further optimization of graphene-modified GFRP systems, bond behavior, and analytical modelling.

THIS PAGE WAS INTENTIONALLY LEFT BLANK

2. STATE OF THE ART

2.1. Materials characterization

2.1.1. Tensile testing

The FRP rebars, especially the GFRP rebars, have come up as an alternative for the use of steel as reinforcement bars due to their tensile strength, non-corrosive nature, lightweight and electromagnetic neutrality. However, the wide application of these materials in structures has not been possible owing to its brittle nature, anisotropic behavior and lesser elastic modulus than that of steel, thus making it necessary for tensile characterization.[9,10].

Typically, the tensile behavior of the GFRP rebars is characterized by three important properties: ultimate tensile strength, elastic modulus, and ultimate tensile strain. The third important property of the tensile behavior of GFRP rebars according to the Canadian code [11] is the Transverse Shear Strength (TSS). However, the accurate estimation of those three properties relies heavily on the chosen method. Unlike steel, the FRP bars cannot be tested through conventional jaws since the application of localized transverse pressure leads to premature fracture of the bar. According to Kocaoz et al. [12], an alternative method for tensile testing of the pultruded GFRP bars involves the use of anchors consisting of steel pipes and expansive cementitious grout. Other researchers decided that inserting some polymer/resin into the steel pipe was a better option (see ASTM discussion below), as this can avoid the problem of slippage of the sample within the testing device.

Despite the extensive popularity of ASTM D7205/D7205M, there are still many other standards available to carry out the tensile tests on FRP rebars, such as ASTM D3916, CAN/CSA-S806, ISO 10406-1, EN 17129, and GOST 31938 [13,14]. Different approaches to anchor selection, gauge length, strain measurements, as well as bar diameter definition result in substantial distinctions of test results. Wiater and Siwowski [13] have found that using “core” instead of “effective” diameter increases tensile strength by 4-16% and elastic modulus by up to 18%, proving that the influence of the test method cannot be ignored.

Apart from the tensile test standards, tensile behavior of GFRP rebars depends heavily on their fiber volume fraction, resin type, orientation of fibers, void fraction, and quality of manufacturing process. You et al. [15] proved that improvements of fibers’ orientation, reduction of voids fraction and fiber pre-

stressing during FRP rebar manufacturing made it possible to achieve tensile strengths of GFRP bars of up to 900 MPa.

In order to overcome problems associated with FRP bars, such as brittle fracture and inadequate ductility, contemporary research efforts are directed towards hybrid bar reinforcement and modification of the matrix system. Zhang and Gao [1] studied a carbon/glass hybrid FRP bar reinforced with graphene-modified polymer matrix at 0.3 weight percent (wt.%) content level and observed an enhancement of 6.9% and 7.1% in initial and ultimate tensile strengths, respectively, along with an improvement in strain capacity and multistage stress-strain curve. This suggests that matrix modification with graphene can improve the properties of hybrid FRP bars.



Figure 1: Failure mode of a) GFRP and b) CFRP rebars [4]

Since the polymer matrix influences stress transfer, crack formation, and fiber-matrix interactions, epoxy modification has been one of the main subjects of research in composite material development. Traditional epoxy resin has been extensively used because of its excellent adhesion and chemical resistance properties, but its brittleness hinders optimal fiber performance. Graphene and graphene nanoplatelets (GNPs) have been widely investigated as nano-fillers because of their high intrinsic modulus, large surface area, and crack-bridging capability [16,17].

Regarding the resin stage, King et al. [18] demonstrated that by incorporating graphene nanoplatelets, the Young's modulus of epoxy can be increased from 2.72 GPa to 3.36 GPa for 6 wt.% loading level, which means an approximate 23.5% increase in the mechanical property. According to Wang et al. [19] smaller graphene platelets usually show better strengthening and stiffening effects when compared to larger platelets; meanwhile, graphene agglomeration at higher loading levels might decrease tensile strength, although it increases stiffness.

Graphene has also shown greater reinforcing efficiency than CNT-based fillers in epoxy systems. Rafiee et al. [20] investigated GNP, single-walled CNTs, and multi-walled CNTs incorporated into epoxy resins at 0.1 wt.% loading level, respectively, and found that graphene has 31% higher Young's modulus and 40% tensile strength increase than the other two counterparts. Similar conclusions have been reported in broader review studies, which attribute the improved efficiency of graphene to its platelet geometry, larger effective contact area, and lower entanglement tendency compared with CNTs [21,22].

In glass fiber composites, the effectiveness of graphene depends strongly on its role within the composite. Topkaya et al. [23] reported that 0.2 wt.% GNP improved the tensile strength and modulus of GFRP composites, confirming the positive effect of low graphene content on fiber-reinforced systems. Dwivedi and Kumar [24] similarly observed that 4 wt.% graphene oxide increased the tensile strength of glass fiber/epoxy composites by 7.46% and elongation by 12.31%, indicating simultaneous improvement in strength and deformation capacity.

There are a few examples of studies where interfacial modification is observed to exhibit remarkable effects on tensile performance. In one such study, Veerakumar et al. [25] showed that functionalized graphene nanoplatelets incorporated on functionalized glass fibers led to an increase in tensile strength of GFRP composites up to 16%. On the other hand, graphene incorporation into the composite matrix yielded more pronounced results in terms of fracture toughness. Another similar study conducted by Kumar et al. [26] also revealed notable enhancements in tensile and interfacial properties of glass fiber composites.

Nevertheless, according to the literature, the introduction of graphene does not always yield positive effects in tensile properties. Poor dispersion, high amount of filler material, and increase in the viscosity of resin may cause poor wetting and stress concentration. Azraai et al. [27] noted that graphene modification of epoxy for pipeline repair, there was no considerable improvement in tensile strength at 2 wt.% of graphene, though there was an increase in ductility. Conversely, Zhang et al. [28] observed 18.5% increase in tensile strength and 22.1% increase in fracture toughness at 0.3 wt.% graphene in a study involving the modification of epoxy vinyl ester resin through graphene and serving as a matrix for composite bars. The overall effect of graphene on FRP strength is summarized below Table 1.

Table 1: Summary table showing the effect of graphene on mechanical properties

Paper	System	Graphene wt.%	Ultimate Tensile Strength	Elastic Modulus	Tensile Strain	Standard
[18]	GNP / epoxy	1–6	-54.3% (6 wt.%)	+23.5% (6 wt.%)	-81.3% (6 wt.%)	ASTM D638
[20]	GPL / epoxy	0.1	+ 40%	+31%	NR	Uniaxial tensile
[29]	Graphene / epoxy vinyl resin	0.1, 0.3, 0.5	+ 18.5% (0.3 wt.%)	+10.8% (0.3 wt.%)	+7.1% (0.3 wt.%)	GB/T 2567-2008
[23]	GNP / GFRP, CFRP, AFRP	0.1–0.3	+ 8.1% (0.2 wt.%)	+7.1–11.6%	NR	ASTM D3039
[24]	GO / GFRP laminate	4	+ 8.1%	NR	-	Not explicitly stated
[28]	GNP / C-G HFRP bar	0.3	+ 4.6–14.9%	≈ No change	+4.4–14.9%	ASTM D7205
[22]	GNPs-coated CF	0.5	+ 14% (mono) / + 71% (multi)	NR	Qualitative increase	GB/T 31290-2014, GB/T 3362-2005
[22]	GNPs/CNTs-coated CFRP	0.5	+ 70%	NR	NR	GB/T 3354-2014

*GNP= Graphene nanoplatelet, GPL= Graphene Platelets, GO= Graphene oxide, NR= Not Reported

The literature indicates that the tensile behavior of GFRP rebars is controlled by the following material parameters. Variation in fiber content, resin/hardener system, mixing method or dispersion quality, voids, and manufacturing process directly influence tensile strength, modulus, and strain, while differences in standards and bar area definitions can significantly alter the reported values [29-31]. At the same time, graphene-modified epoxy systems have demonstrated strong potential to improve stiffness, crack resistance, and fiber-matrix stress transfer in both neat resin and glass fiber composites [18], [28], [32]. The degree of improvement, however, remains highly dependent on graphene type, dosage, functionalization, and dispersion route as summarized in Table 1 above. These findings establish a clear basis for evaluating the tensile performance of GFRP rebars manufactured with conventional epoxy and graphene-modified epoxy matrices under standardized direct tensile testing.

2.1.2. Transverse Shear Strength (TSS) Testing

As opposed to the longitudinal tensile behavior of GFRP bars that depend on the reinforcing fibers, the TSS is mainly dependent on the polymer matrix and the fiber-matrix interface. The load transfer process

during transverse loading occurs through the resin-rich areas where the stresses between adjacent fibers get transmitted. Hence, the matrix and the fiber-matrix interface become the key aspects that control the TSS. As such, TSS becomes a measure of the structural integrity of the FRP composites. GFRP bars used in reinforced concrete structures can be subjected to transverse shear stresses as a result of dowels, anchorages, connectors, bent reinforcements, and other shear transfer mechanisms. That is why a standardized double shear test has been developed as specified in ASTM D7617/D7617M [33,34].

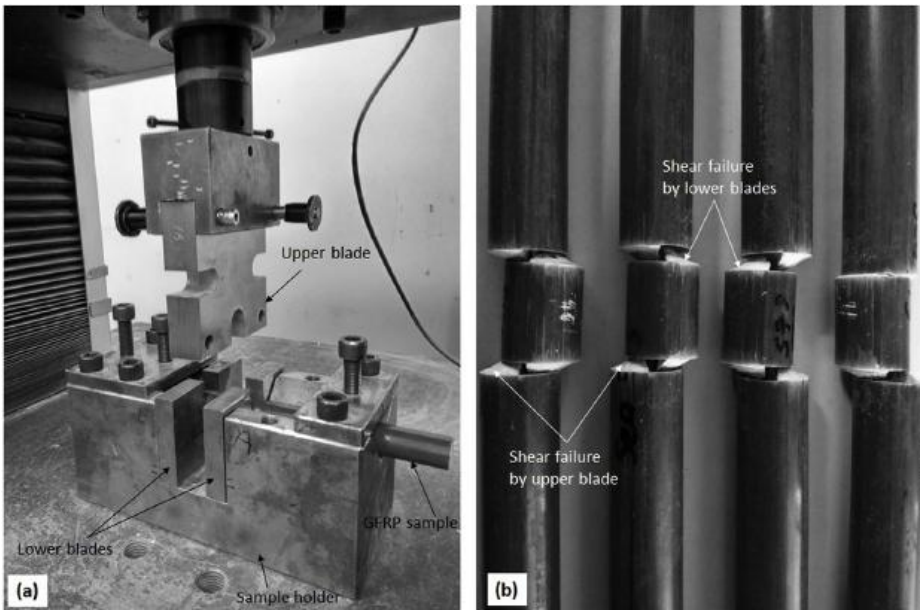


Figure 2: (a). Transverse shear testing set-up (b). Failure mode of GFRP rebars [35]

Transverse shear characteristics of GFRP bars are controlled by several parameters, such as fiber arrangement, reinforcing pattern, shape of the bar surface, as well as matrix properties. According to Gao et al., increasing rib depth improved the transverse shear strength from 247.9 MPa to 263.5 MPa, while increased rib spacing lowered the ultimate shear strain. Moreover, Gao et al.[36] found out that fiber arrangement and hybrid reinforcement have an important impact on shear strength, which makes stress transfer inside the composite very essential. Similar results were obtained by Genikomsou et al [37]., who stated that transverse shear testing is an effective tool for assessing internal quality of the material because removing the outer layer had no impact on shear strength. It means that transverse shear strength of GFRP bars depends more on their inner composite structure and fiber/matrix interface than on the surface treatment.

The durability of the polymer matrix is another factor that contributes significantly to ensuring good transverse shear strength. According to Sawpan [38], GFRP bars exhibited about 91% of their original

transverse shear strength after 20 months of exposure to seawater at 75°C, and the drop in strength was due primarily to the degradation of the matrix and fiber-matrix debonding instead of fiber degradation. The results indicate that the transverse shear behavior is very susceptible to the resistance of the polymer matrix, and thus enhancing matrix properties will improve shear strength.

Given the matrix-dominated behavior of transverse shear failure, recent research has been directed at the use of nanomaterials within polymer resins for strengthening interfacial bond and mechanical properties. Ogrodowska and Urbański [39] found that using 3 wt.% of nanosilica to modify an epoxy resin improves fiber-matrix interphase and increases both elastic modulus and thermal stability of hybrid FRP bars. Similarly, Alaei et al. [40] found that addition of 0.25 wt.% of graphene nanoplatelets (GNPs) to vinyl ester based GFRP bars not only increased transverse shear strength by 6% but also interlaminar shear strength by 10%. Moreover, the use of GNPs reduced the water absorption rate by 43% and retained 97% of its original shear strength even after alkaline immersion. Graphene nanosheet (GNS) modification enhanced the transverse shear strength of carbon/glass composite FRP tendons by 40.9% on average due to enhanced crack bridging, interfacial bonding and stress transfer [41]. It can be seen from these studies that matrix modification using graphene-based nanomaterials can successfully address the problem of interfacial defects and improve the transverse shear strength of the materials. Graphene-modified epoxy GFRP reinforcing bars have been studied insufficiently until now. As transverse shear behavior is mainly dependent on the polymer matrix and fiber-matrix interface, testing transverse shear strength of graphene-modified epoxy GFRP bars would allow for the evaluation of the effectiveness of graphene introduction and will complement tensile and bond-strength studies discussed in this thesis.

2.2. Concrete bond performance

The behavior of bond between glass fiber reinforced polymer (GFRP) reinforcing bars and concrete is among the governing factors affecting the performance of FRP-reinforced concrete structures. In contrast to steel reinforcements, GFRP bars display anisotropic behavior, lower modulus of elasticity, and linear-elastic stress–strain behavior up to failure. For this reason, the process of force transmission between GFRP reinforcement and concrete is completely different from steel reinforcement. Good bond behavior is very important for ensuring good stress transfer, crack control, and anchorage performance of FRP-reinforced concrete structures throughout their entire lifetime [42], [43].

The bond between GFRP bars and concrete is generally developed through three primary mechanisms: chemical adhesion, friction, and mechanical interlock as shown in Figure 3. Chemical adhesion governs

the initial stage of loading and is associated with the bonding between the polymer surface and hydrated cement paste. As loading increases, adhesion is progressively lost and frictional resistance develops due to relative movement between the bar and surrounding concrete. Mechanical interlock, which is generated through surface deformations such as ribs, grooves, helically wrapped fibers, sand coatings, or surface indentations, is generally considered the dominant bond mechanism in commercial GFRP bars [3], [42], [44]. The contribution of each mechanism depends on the bar surface configuration, matrix characteristics, concrete properties, and confinement conditions.

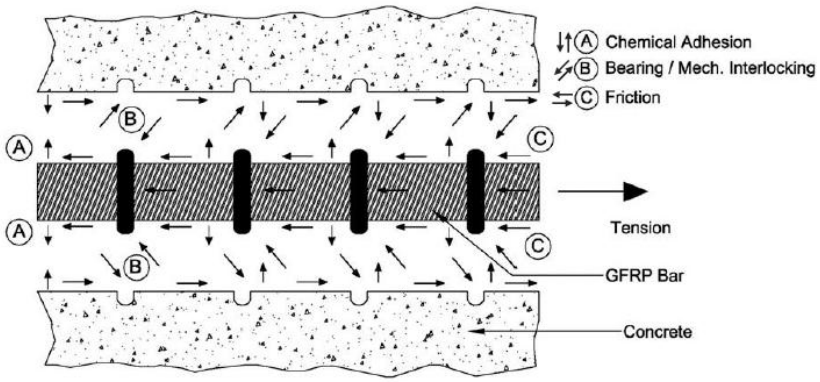


Figure 3: Bond stress transfer mechanism between GFRP bar and concrete [3]

Characterization of the bond behavior of GFRP bars is normally achieved using bond-slip relations established using the direct pull-out test. Bond-slip relations are usually plotted as an ascending section, a peak bond stress region, and then a descending section, which indicates increasing debonding and friction. At low loads, the adhesion between the two materials and micro-mechanical interlock govern the behavior. When the load continues to rise, damage occurs to the interface and results in peak bond stress. After reaching the peak bond stress, debonding of the two materials takes place; hence, bond stress decreases with an increase in slip. The residual bond behavior is governed by friction and micro-mechanical interlock [45], [46]

2.2.1. Surface treatment / features:

Various studies have attempted to study the effect of surface treatment on the bond behavior of GFRP bars. Surface characteristics have proved to be one of the main factors affecting bond strength and failure mechanism. Sand-coated bars create high surface roughness and good adhesion at the early stages of the applied loads; however, there is a risk of reducing the bond capacity due to the separation of sand particles from the resin surface. Bond capacities are usually higher for ribbed and helically wrapped bars due to mechanical interaction between these bars and the surrounding concrete matrix. It has been

proven through experiments that ribbed bars can have bond capacities similar to those of steel reinforcements in confined concrete specimens, while smooth bars show significantly lower bond capacities [45], [47], [48]. Figure 4 presents commercially used FRP rebars of various surface forms.

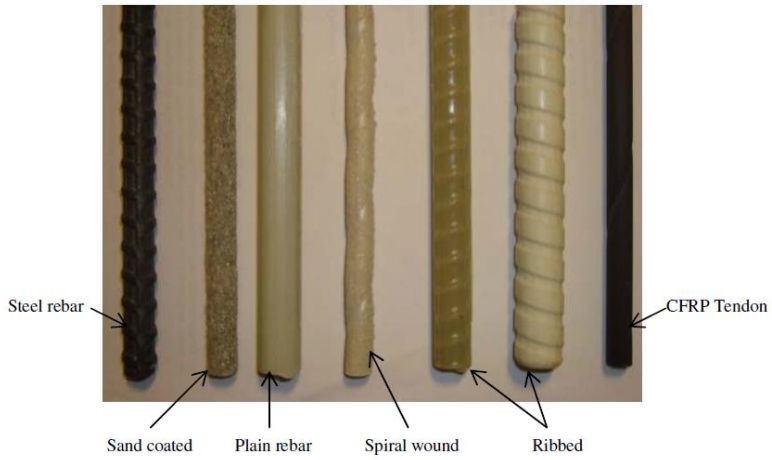


Figure 4: Different types of commercially available FRP rebars*[49]*

Studies carried out with respect to helically wound GFRP bars in UHPC showed that the good mechanical interlock created by the presence of surface deformation along with the ability of UHPC to create a high level of confinement led to significant advancements in terms of bond characteristics. Bond failures in the UHPC system were found to occur due to localized failure of the GFRP surface rather than concrete failure, which signifies that the bond strength was governed by the interface itself. This is additional evidence that matrix behavior and surface treatments govern bond performance for high strength concrete systems [50].

2.2.2. Bar diameter:

There has been much consideration for the effect of bar diameter in literature. Majority of the studies observed that there is a reduction in the average bond strength when there was an increase in the bar diameter. The reason for this could be due to the uneven distribution of bond stress and confinement efficiency, as well as the possibility of defects during the manufacturing process. Smaller diameter bars have been noted to display high bond efficiency since the stresses were evenly distributed throughout the bonded length. Baena et al. concluded that an increase in bar diameter led to a decrease in average bond strength regardless of the surface treatment method used [46]. Similar observations have been studied and reported in subsequent experimental studies and analytical reviews [42], [51].

2.2.3. Bond length:

Bond (Embedment) length is another major factor that affects bond behavior. Several studies have shown that increase in the embedment length causes an increase in the pull-out resistance but causes a decrease in the average bond stress since the stress distribution becomes less uniform for longer bond lengths. For longer bond lengths, there are stresses at the loaded end; therefore, their bond efficiencies decrease. Increase in the embedment length also increases energy dissipation and slip resistance but decreases the average bond stress [43], [52].

2.2.4. Concrete compressive strength:

Several studies have shown that there is a positive relationship between the compressive strength of concrete and bond strength. The higher compressive strength makes the concrete more resistant to local crushing and radial stresses due to deformations of the bars. On the other hand, there are some studies finding that beyond around 30 to 40 MPa, increasing the strength of concrete does not lead to significant improvements in bond strength, as the limiting factor is no longer concrete crushing but interfacial damage near the FRP surface [50], [52,53].

2.2.5. Concrete confinement:

Concrete cover and confinement levels have a great influence on the bond characteristics and failure mechanism. Proper confinement controls crack growth radially and postpone splitting failure; thus, the interface is able to sustain high bond stress values. In specimens with insufficient cover depth, radial stresses created under load can cause early splitting of concrete before complete utilization of bond strength. Transverse reinforcements, fibers, or any form of confinement system contribute positively to bond behavior by restraining crack development and confining pressure of reinforcement [47], [54].
Reported failure mechanisms from the available literature include pull-out, splitting, and surface damage failure types. Pull-out failure is normally linked to proper confinement level and involves gradual debonding along the bonding interface. When the induced radial stress exceeds tensile strength of concrete, splitting failure happens and causes longitudinal cracks along with bond failure. Surface damage of GFRP bars that includes rib shearing, separation of sand coating, or delamination of polymer layer is another type of failure. Determination of failure mechanisms largely depends on a combination of several factors such as reinforcement bar dimensions, concrete, length of embedment, and confinement level [42], [46]

2.2.6. Environment/Temperature:

The resistance of the composite formed by the interaction of the GFRP bars and the concrete against the effects of the environment is one of the essential topics for researchers as more and more FRPs are used as reinforcements in harsh environments. GFRP bars placed in concrete undergo the influence of alkalinity, wetting/drying cycle, freezing/thawing, thermal cycling, and high temperatures. Such factors can affect the interface between fibers and the matrix and, therefore, change the properties of the composite bond. The effect of elevated temperatures deserves particular attention, as the polymer matrix softens near the glass transition temperature. It was proven experimentally that bond strength dropped significantly above the glass transition temperature of the conventional polymer matrix. Therefore, the stability of the matrix is of paramount importance [42], [45].

There has been considerable attention focused on sustainable concrete systems reinforced by GFRP bars over recent years. Studies on bond properties have been done on seawater concrete, recycled aggregate concrete, Limestone Calcined Clay Cement (LCC), Ultra-High-Performance Concrete (UHPC), and Ultra-High-Performance Fiber-Reinforced Concrete (UHPFRC). While there is a difference in the material composition, research suggests that GFRP bars show satisfactory bond performance with proper surface treatment and confinement. The sustainable concrete system showed bond strength similar to conventional concrete while providing added environmental benefits [43], [54].

Besides regular concrete, recent works have also shown an increasing interest in studying the bond performance of GFRP bars in advanced cement composites, like UHPC and UHPFRC, which are characterized by higher tensile and compressive strengths, as well as higher resistance against environmental degradation, than those of regular concrete. The denser microstructure, along with the increased confinement effect created by adding steel or synthetic fibers, can provide better interface interaction between the GFRP bars and cement composites. Some studies found that UHPC specimens demonstrated higher peak bond stress levels, as well as better post-peak behavior, than specimens made from normal concrete [50], [53].

In order to describe the behavior of GFRP bars within concrete, various bond slip models have been suggested. The most popular ones include the Bertero–Popov–Eligehausen (BPE) bond-slip model, the modified BPE bond-slip model, the Cosenza–Manfredi–Realfonzo (CMR) bond-slip model, and different empirical models based on the pull-out test data. All those models try to describe the ascending part of the slip curve, its peak, and its descending branch. While different models work well under certain circumstances, no universal bond-slip model has been found that would be suitable for all GFRP systems

because bond characteristics depend significantly on such parameters as surface geometry, composite material type, concrete strength, and confinement [46], [55].

2.2.7. Matrix modification:

While there has been much research carried out on traditional GFRP bars, recent studies have focused on the development of better materials for the polymer matrix. The polymer matrix is essential for ensuring proper fiber orientation, load transfer between fibers, fiber protection from the environment, and the maintenance of surface deformation features. Currently, some of the most frequently used polymers in commercial GFRP bars include epoxy, vinyl ester, and polyester resins. In terms of performance, epoxy is known to outperform other resins in terms of mechanical strength, thermal resistance, low shrinkage rate, and good fiber adhesion. Nevertheless, the high price of epoxy resin has led researchers to seek new solutions for improving inexpensive polymers [43].

Nanotechnology has emerged as one of the most promising approaches for improving the mechanical and durability performance of polymer composites. Nanomaterials such as nano-silica, nano-titania, carbon nanotubes (CNTs), and graphene nanoplatelets (GNPs) have demonstrated significant potential for enhancing matrix properties. These nanomaterials possess extremely high surface areas and exceptional mechanical characteristics, allowing them to interact effectively with the polymer network. Their incorporation into polymer matrices can improve stiffness, fracture toughness, crack resistance, thermal stability, and interfacial bonding [56].

Research on nanomaterial-modified concrete systems has shown that nanomaterials can significantly improve the bond between FRP bars and concrete. The microstructural study showed that nanomaterials help in refining the hydrates, lowering porosity and increasing the density of interfacial transition zone of FRP bars. According to Wang et al., adding nanomaterials enhances the bonding strength of GFRP bars to 16.2%, along with lowering the slip at maximum load and increasing the residual bonding strength [56]. The scanning electron microscope studies also suggested that nanomaterials helped in decreasing the number of defects in the duplex film area, which is considered the most vulnerable part regarding interfacial failure.

Graphene is considered one of the most promising nanomaterials due to the excellent properties such as mechanical, thermal, and physical characteristics that make this material unique. This material demonstrates an elasticity modulus close to 1 TPa and high strength that outperforms most engineering materials, and in addition, this material is light. Graphene nanoplatelets are easily added to the polymer composites in small amounts and prove their efficiency as fillers. It has been proved that graphene is

preferable to use as filler instead of carbon nanotubes in polymer composites because it is less expensive, more convenient to handle, and better dispersed within polymer system [43].

Main mechanisms of graphene effect on polymer properties are described as crack bridging, crack deflection, load transfer improvement, and restriction of polymer chain movement. Due to these mechanisms, stiffness of polymer matrix increases, while number of microcracks decreases. The improvement of adhesion between fibers and matrix results in more effective transfer of loads from matrix to the fibers and increase of composite mechanical properties. Also, graphene promotes thermal stability of the material [57].

Though there is extensive literature on graphene-polymer nanocomposites, only limited research has focused on the effect of graphene modification on the bonding properties of FRP reinforcement bars within concrete structures. In one of the notable works related to this topic, Bueno and Bittencourt evaluated the bonding properties of graphene-enhanced polymeric matrix material used for manufacturing FRP bars undergoing pull-out testing. It was found that the addition of graphene had enhanced the bonding properties of polyester FRP reinforcement bars by up to 49% at ambient temperatures and also had reduced the degradation of bonding characteristics under high temperatures [43]. This shows that graphene has the ability to overcome the weaknesses of existing polyester matrix materials.

The second crucial findings from these studies on graphene-based bonds is the enhancement of thermal resistance. Traditional polymer-based matrices suffer great losses in terms of stiffness and bond capability when subjected to elevated temperatures close to the glass transition point. The graphene-based matrices revealed reduced bond loss and better capability of maintaining their bond capability when subjected to high temperatures. This is because graphene nanoplatelets were able to minimize the movement of polymer chains at higher temperatures. In this respect, graphene-based bonds can become a good solution to increase the fire resistance of GFRP reinforcement [43], [57].

Despite the encouraging findings obtained from experimental work carried out to date, there are still many gaps in existing knowledge regarding graphene modification of bonds. Specifically, several research studies concerning graphene have been carried out on tensile, flexural, and thermal properties of polymer composite materials rather than their bond characteristics. Moreover, while some research has been conducted to examine the influence of graphene on GFRP bar bond, most such experiments have involved consideration of only one graphene dosage level. The impact of graphene dosage level, dispersion quality, bar size, surface condition, embedment length, and concrete strength has yet to be established.

[49] shows that considerable advancements have been made in the field of bond characteristics of GFRP bars. Factors such as surface preparation, bar diameter, embedment length, concrete grade,

confinement, and environmental effects have been recognized as factors affecting bond performance. However, recent innovations in the area of UHPC, sustainable concrete technology, and nanoparticle reinforcement of composite materials have widened the scope of study on FRP-concrete interaction phenomena. It is noted that little comparative research has been conducted between the bond characteristics of traditional epoxy-embedded GFRP bars and graphene-reinforced epoxy matrices. Therefore, further experimental investigation is required to establish the effectiveness of graphene modification in enhancing bond performance and to support the development of reliable design recommendations for future GFRP-reinforced concrete structures. Following table shows a summary of the effect of nanomaterial modified matrix on the GFRP-concrete bond performance. Table 2 summarizes the findings reported in the literature regarding the effects of different nanomaterials incorporated into the polymer matrix on the bond performance of GFRP reinforcing bars with concrete.

Table 2: Effect of nanomaterials matrix modification on rebar-concrete bond performance

Reference	Nanomaterial	Key Bond Result
Wang et al. [56]	Nano-silica (NS), Nano-titania (NT), Carbon nanotubes (CNTs), Multilayer Graphene (MLG)	Bond strength +16-42%
Bueno and Bittencourt [43]	Graphene-enriched polymer	Bond strength +49%
Al-Zu'bi [57]	Graphene/CNT-modified epoxy	Improved adhesion, toughness, and stress transfer

THIS PAGE WAS INTENTIONALLY LEFT BLANK

3. EXPERIMENTAL CAMPAIGN

This chapter highlights the sample preparation and experimental methodology used in this study. Sample preparation and manufacturing process of both the conventional and graphene reinforced GFRP bars, as well as the preparation process of the concrete samples to be used in bond tests are included in this section. This chapter describes the experimental program developed to test the performance of GFRP bars in terms of materials characterization i.e. tensile strength, transverse shear strength and concrete-GFRP bar bond performance. All experimental procedures, specimen configuration, loading conditions, measurement processes and data analysis are done following the guidelines of the respective ASTM standards for each test. The nomenclature of specimen used for materials characterization is CE/GE_X where CE and GE mean conventional epoxy and graphene-modified epoxy respectively while X represents the bar diameter (6,8 or 12 mm). For the direct pull-out test CE/GE/S_5Ø or 10Ø is used where CE and GE has same meaning as previously defined, S is used for Schock company rebar which is taken as a benchmark, while 5Ø and 10Ø represent bond length which is 60 mm and 120 mm respectively as the bond test is performed only for the 12mm diameter rebar.

The graphene content incorporated into the epoxy matrix was maintained at less than 1 wt.%. The precise graphene dosage cannot be disclosed due to confidentiality restrictions by the Portuguese supplying company (GRUN). Therefore, the present study focuses on evaluating the effect of graphene modification rather than the influence of its specific concentration.

3.1. Materials characterization

3.1.1. Tensile testing

The experimental variables considered in this test were the matrix type and the bar diameter. Conventional epoxy and graphene-modified epoxy GFRP reinforcing bars with nominal diameters of 6 mm and 8 mm (received from the Portuguese company GRUN, manufactured via pultrusion process) were investigated to evaluate the influence of graphene incorporation on the tensile performance of the composite reinforcement. For each specimen category, two identical specimens were tested to ensure the repeatability of the experimental results. Below table 3 summarizes the experimental program adopted for Mechanical testing.

Table 3: Variables and scheme for mechanical testing

Series	Matrix	Bar Diameter	No. of Specimens	Purpose
CE_6	Conventional epoxy	6 mm	2	Reference specimen
GE_6	Graphene-modified epoxy	6 mm	2	Effect of graphene
CE_8	Conventional epoxy	8 mm	2	Reference specimen
GE_8	Graphene-modified epoxy	8 mm	2	Effect of graphene

The mechanical properties of the GFRP reinforcing bars were determined according to the ASTM D7205/D7205M [14], Standard test method for tensile properties of fiber reinforced polymer matrix bars with a modification in sample length due to the constraint of the MTS machine. The test was conducted to evaluate the influence of graphene-modified epoxy on the tensile behavior of GFRP reinforcing bars by comparing their tensile strength, elastic modulus, strain at failure, and failure modes with those of conventional epoxy GFRP bars.

Each specimen had a total length of 450 mm, consisting of a 150 mm steel anchorage (18 mm diameter with 2 mm thickness) at each end and a 150 mm free gauge length between the anchorages. The steel tubes were used for anchorage systems so that uniform load transfer could be achieved from the testing machine to the GFRP bars while preventing premature gripping failure. Bonding of the GFRP bars within the steel tubes was achieved through S&P Resin 220 epoxy adhesive. The bonding was done according to the instructions by the manufacturer of the resin material. The tensile test specimen configuration and the experimental setup are illustrated in Figure 5 below.

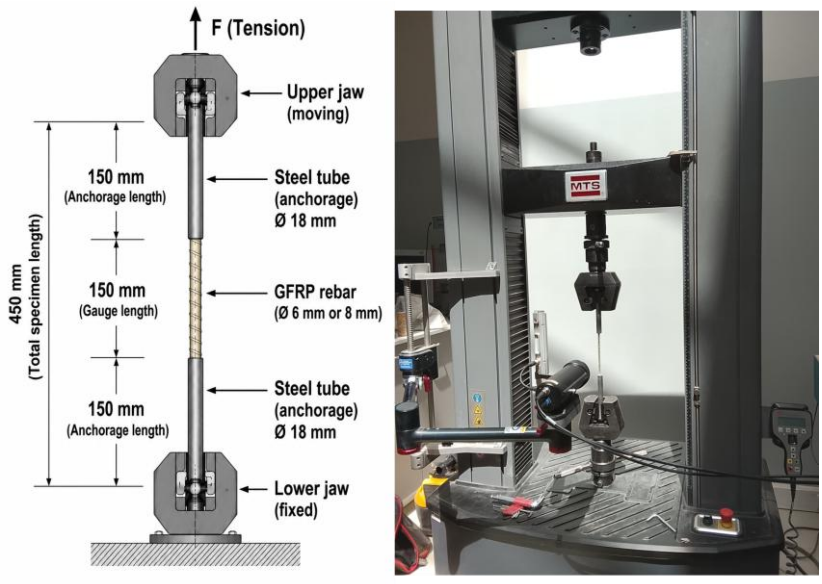


Figure 5: Mechanical testing schematics and photo of the test

The tensile tests were conducted using MTS tensile testing machine equipped with an appropriate load cell of maximum capacity of 100kN under displacement-controlled loading condition with the loading rate specified in ASTM D7205/D7205M [14]. The applied tensile load and corresponding displacement (via DIC camera optical extensometer) were continuously recorded throughout the test until specimen failure. The maximum tensile load was used to calculate the ultimate tensile strength, while the stress–strain response was used to determine the elastic modulus and ultimate tensile strain according to the recommendations and formulas mentioned in ASTM D7205/D7205M standard [14].

After conducting the test, the failure modes of each sample were analyzed to ensure that they met the requirements for failure according to the standard and to investigate the effect of graphene addition on the tensile failure mode. The tensile performance of the conventional epoxy and graphene-modified epoxy GFRP bars was then compared in terms of ultimate tensile strength, elastic modulus, ultimate tensile strain, and failure characteristics.

3.1.2. Transverse Shear Strength (TSS) testing

The transverse shear strength (TSS) of the GFRP reinforcing bars was evaluated in accordance with ASTM D7617/D7617M-11 [34] using a double-shear fixture mounted on a Universal Testing Machine (UTM). This test was performed to investigate the effect and influence of graphene-modified epoxy on the transverse shear performance of GFRP reinforcing bars. Since the transverse shear behavior of GFRP bars is primarily governed by the polymer matrix and the fiber–matrix interface, it provides an effective means of evaluating the influence of graphene incorporation on the matrix-dominated mechanical properties of the composite. The schematic illustration of the test configuration and the corresponding experimental setup adopted in the present study are shown in Figure 6 below.

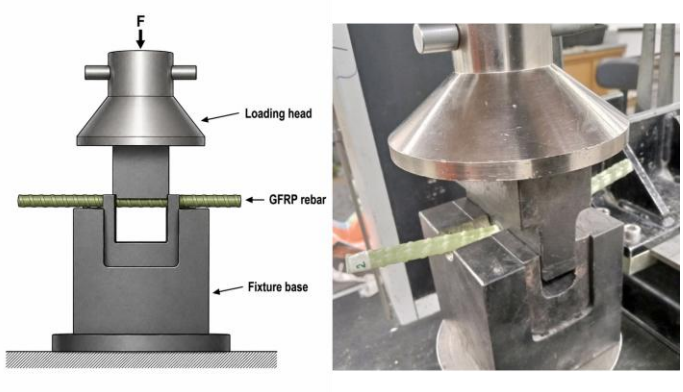


Figure 6: Transverse shear strength test schematics and photo of the test

Conventional epoxy and graphene-modified epoxy GFRP reinforcing bars with nominal diameters of 6 mm, 8 mm, and 12 mm were investigated. The GFRP bars were cut into 225 mm long specimens in accordance with the requirements of ASTM D7617/D7617M-11 [34]. For each bar diameter and material configuration, five specimens were tested to ensure the repeatability and reliability of the experimental results.

Each specimen was carefully positioned in the double-shear fixture to ensure proper alignment before testing. The tests were performed under displacement-controlled loading, and the loading rate was selected in accordance with ASTM D7617/D7617M-11 to ensure specimen failure within the time interval specified by the standard. During testing, the applied load and crosshead displacement were continuously recorded until complete specimen failure.

The transverse shear strength was calculated from the maximum failure load using the equation specified in ASTM D7617/D7617M-11 [34]:

$$\tau_u = \frac{P_s}{2A} \tag{3.1}$$

where τ_u is the transverse shear strength (MPa), P_s is the maximum failure load (N), and A is the nominal cross-sectional area of the GFRP reinforcing bar (mm^2).

The evaluation of transverse shear properties of the conventional epoxy and graphene-modified epoxy GFRP reinforcement bars was done through comparison of their ultimate transverse shear strength and failure modes, specifically with respect to the effects of graphene on matrix dominated nature of the reinforcement material.

3.2. Concrete bond performance

The experimental variables used in this research work are the epoxy matrix and bond length. The two bond lengths used were 5Ø and 10Ø in order to determine the effect of embedment length on the bond behavior of GFRP bars. Furthermore, a comparison was made between traditional epoxy GFRP bars and graphene added epoxy GFRP bars to find out the effect of graphene addition to the epoxy matrix. Schöck rebars [58] (from German company and commercially available in market) with a bond length of 5Ø were also tested as benchmark specimens for comparison with the GFRP rebar from GRUN. For each test

configuration, two identical specimens were prepared and tested for each series. Below Table 4 summarizes the experimental program adopted for the direct pull-out tests.

Table 4: Summary of variables for pull-out test

Series	Matrix	No. of Specimens	Purpose
S_5Ø	Vinyl ester	2	Benchmark specimen
CE-5Ø	Conventional epoxy	2	Reference GFRP
GE-5Ø	Graphene-modified epoxy	2	Effect of graphene
CE-10Ø	Conventional epoxy	2	Effect of bond length
GE-10Ø	Graphene-modified epoxy	2	Combined effect of graphene and bond length

Prior to concrete casting, the GFRP bars were positioned and aligned within the formwork, as illustrated in Figure 7(a). PVC tubes were placed around the rebars to isolate the unbonded region and to ensure that the interaction between the GFRP bar and concrete occurred only along the predefined bonded length of 5Ø (60 mm) or 10Ø (120 mm). Particular attention was given to maintaining the position of the bars during casting and to sealing the passages through the formwork to prevent concrete leakage and displacement of the specimens as shown in Figure 7(b).

The concrete was then placed into the moulds and mechanically compacted using an internal vibrator to reduce entrapped air and ensure adequate consolidation around the GFRP bars, as shown in Figures 7(c) and 7(d). After casting, the exposed concrete surfaces were levelled, and the specimens were maintained under the adopted curing conditions before being transferred to the laboratory. The pull-out tests were performed after a total curing period of 28 days.

Prior to testing, steel tube anchorages were prepared at the loaded end of the GFRP bars using the same anchorage concept adopted for the tensile specimens. The bars were centered within the steel tubes and bonded using S&P Resin 220 epoxy adhesive to provide adequate load transfer from the testing machine to the GFRP reinforcement and to prevent premature gripping failure. Figure 7(e) shows the preparation of the steel tube anchorage, while Figure 7(f) presents the pull-out specimens after anchorage installation and prior to testing.



(a) (b)

(c) (d)

(e) (f)

Figure 7: Preparation of direct pull-out specimens: (a) positioning of GFRP bars and PVC sleeves in the formwork; (b) fixation and sealing of the bars prior to casting; (c) concrete casting; (d) concrete compaction using an internal vibrator; (e) and (f) preparation of testing

The bond behavior between GFRP reinforcing bars and concrete was evaluated through direct pull-out tests (DPT) in accordance with ASTM D7913/D7913M [8]. The specimens consisted of 12 mm diameter ribbed GFRP bars centrally embedded in 200 mm × 200 mm × 200 mm concrete cubes. As mentioned

before, two embedment lengths, corresponding to 5Ø (60 mm) and 10Ø (120 mm), were adopted. The remaining embedded portion of the bar was isolated using a PVC pipe to eliminate bond outside the intended bonded region, ensuring that load transfer occurred only within the specified anchorage length. The concrete was casted according to the ACI standard and left for 10 days at construction site which later shifted to the lab for putting steel tube anchorages (same as used for tensile test samples). A total of 28 days were given (according to the standard) for the samples. Three standard cubic (150x150x150 mm^3) specimens for concrete compressive strength were also casted and then tested (after 28 days) and the strength found 25.1 MPa (concrete class: C20/25). The schematic illustration and the experimental setup adopted for direct pull-out test are shown in Figure. 8. (a) and Fig. 8. (b), respectively.

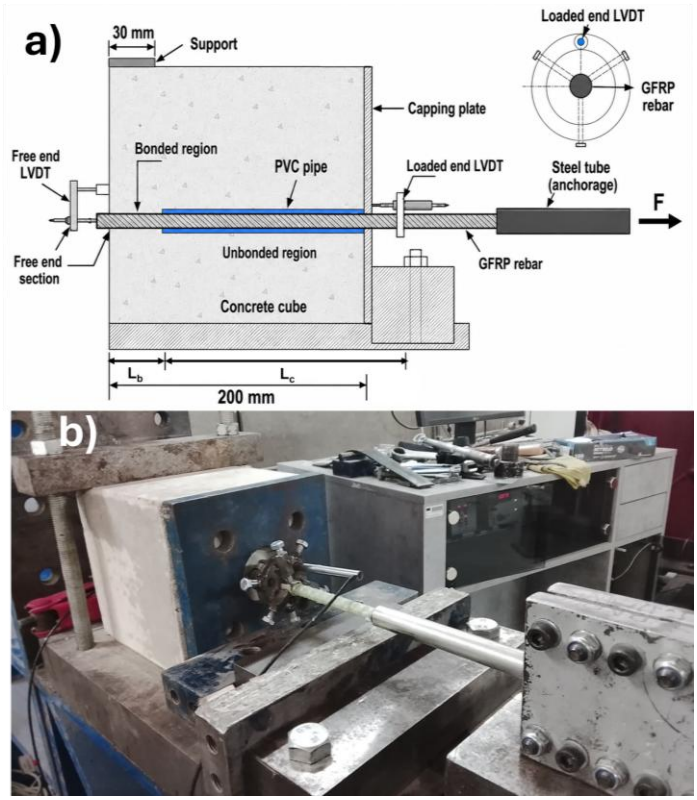


Figure 8: Pull-out test setup a) Schematics and b) photo of the test

The pull-out tests were performed using a testing frame at the structural laboratory of civil engineering department in University of Minho with the testing frame of loading capacity of 300kN under displacement-controlled loading at a constant loading rate of 0.021 mm/s, following the recommendations of ASTM D7913/D7913M [8]. The applied pull-out load was continuously recorded using the machine load cell.

The relative displacement between the GFRP rebar and concrete was recorded using two Linear Variable Differential Transformers (LVDTs) positioned parallel to the loading direction. One LVDT was installed at the loaded end, where it was attached to the GFRP bar through a circular clamp while its probe remained in contact with the concrete surface to measure the loaded-end slip. The second LVDT was positioned at the free end, with its probe directly contacting the free end of the GFRP bar to record the corresponding free-end slip. The arrangement of the LVDTs is illustrated in Figure 8. During each test, the applied load and the corresponding slips at both the loaded and free ends were continuously recorded until bond failure occurred and the specimen freely slipped. The average bond stress was determined according to ASTM D7913/D7913M [8] using the formulas discussed in the results and discussion chapter of this thesis.

The bond performance of conventional epoxy GFRP bars, graphene-modified epoxy GFRP bars, and benchmark Schock rebar were subsequently evaluated by comparing the bond stress-slip response, ultimate bond strength, bond stiffness, and failure modes. Particular emphasis was placed on assessing the influence of graphene modification and embedment length on the bond characteristics between the reinforcement and surrounding concrete.

4. Results and Discussion

This section presents and discusses the results obtained from the experimental characterization of the GFRP rebars and their bond performance with concrete. The specimen nomenclature adopted throughout this chapter follows that previously defined in Chapter 3, where the experimental campaign, specimen configurations, and testing procedures were described.

4.1. Materials characterization

4.1.1. Tensile testing

Figure 9 shows the stress-strain curves of the CE and GE GFRP rebars having 6 and 8 mm diameters. Two specimens for each series were used, and their average values were graphed. As seen from the figure, all specimens exhibit a linear relationship until they reach failure, beyond which there is an abrupt reduction in stress values, thus indicating the brittle nature of tensile failure of the reinforcement. The lack of yielding zone signifies that the deformation process has been entirely elastic before failure, which is the case with the usual results reported in the literature. The corresponding tensile strength, tensile strain, and elastic modulus are summarized in Table 5.

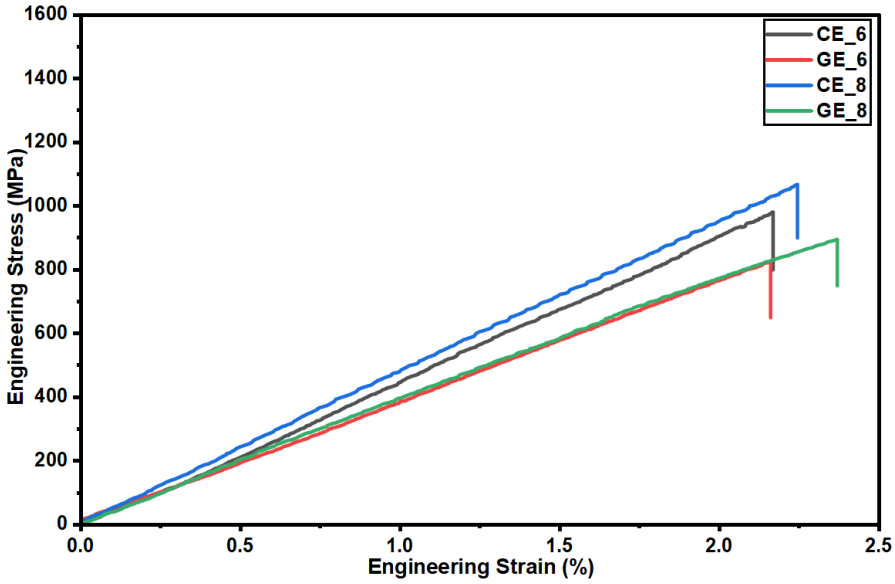


Figure 9: Tensile test experimental results

Table 5: Summary of the tensile test results

Series	Tensile strength (MPa)	Tensile strain (%)	Elastic Modulus (GPa)
CE_6	981.0	2.16	38.1
GE_6	825.8	2.16	34.7
CE_8	1068.3	2.24	46.7
GE_8	895.3	2.36	39.2

The increase in diameter of the bar from 6 mm to 8 mm improved the tensile behavior of the specimens of both epoxy types. The tensile strength of conventional epoxy increased from 981 MPa (CE_6) to 1068.3 MPa (CE_8) and the elastic modulus from 38.1 to 46.7 GPa, respectively. In the same manner, the increase in the tensile strength of the graphene-filled specimens went from 825.8 MPa (GE_6) to 895.3 MPa (GE_8) and their elastic modulus from 34.7 to 39.2 GPa. Based on the increase in both properties, the larger bar specimens had better tensile stiffness and load capacity. Nonetheless, the increase in the tensile strength was rather small when compared with the increase in elastic modulus, showing that diameter had a greater influence on stiffness than tensile strength.

On the other hand, comparing the same rebar diameter reveals that addition of graphene in the epoxy matrix leads to a decrease in the tensile strength and elastic modulus. In the case of 6 mm diameter rebars, there was a decrease in tensile strength from 981 MPa in CE_6 to 825.8 MPa in GE_6, which corresponds to a decrease of about 15.8%, while the elastic modulus was decreased by about 9.0%. In the case of 8 mm rebars, the tensile strength decreased from 1068.36 MPa in CE_8 to 895.3 MPa in GE_8, which corresponds to a decrease of about 16.2%, while the elastic modulus decreased from 46.7 to 39.2 GPa. The similar decrease in tensile strength for both diameters indicates that the observed phenomenon does not depend much on the diameter but on the changed polymer matrix.

For comparison, Soares et al. [52] reported an average tensile strength of 1527.9 MPa and an elastic modulus of 69.0 GPa for Ø8 Schöck ComBAR GFRP rebars. These values are higher than those obtained in the present study for the same nominal diameter, where CE_8 exhibited a tensile strength of 1068.36 MPa and an elastic modulus of 46.73 GPa, while GE_8 reached 895.3 MPa and 39.2 GPa, respectively. Compared with the Schöck rebar, this corresponds to reductions of approximately 30% in tensile strength and 32% in elastic modulus for CE_8, and approximately 41% and 43%, respectively, for GE_8.

Nevertheless, this comparison should be interpreted with caution. The Schöck and GRUN rebars correspond to different GFRP systems, including differences in resin type, fiber content, manufacturing

process and surface configuration. Furthermore, due to laboratory constraints and the unavailability of the tensile testing machine previously used for this type of characterization, the experimental setup adopted in the present study had to be adapted, including a reduction of the specimen length to comply with the available MTS testing machine. Consequently, the differences observed cannot be attributed exclusively to the material composition or to the graphene modification, since the differences between the GFRP systems and the adapted experimental configuration may also have influenced the measured tensile properties.

The lower tensile properties observed for the graphene-modified specimens, as well as the differences identified when compared with the Schöck reference values, do not necessarily indicate an intrinsically negative effect of graphene on the reinforcement system. Instead, it means that, for the current graphene amount, dispersion state, and manufacturing conditions used in the current work, the modified material does not show any significant improvement in fiber-to-matrix stress transfer. Effects including volume fraction of the fibers, non-uniform distribution of graphene, agglomerations or changes in matrix properties might lead to stress concentration and decrease in stress transfer efficiency between the matrix and fibers. These hypotheses cannot be proved by the tensile test data only, so they can be considered as possible options but not as conclusive evidence.

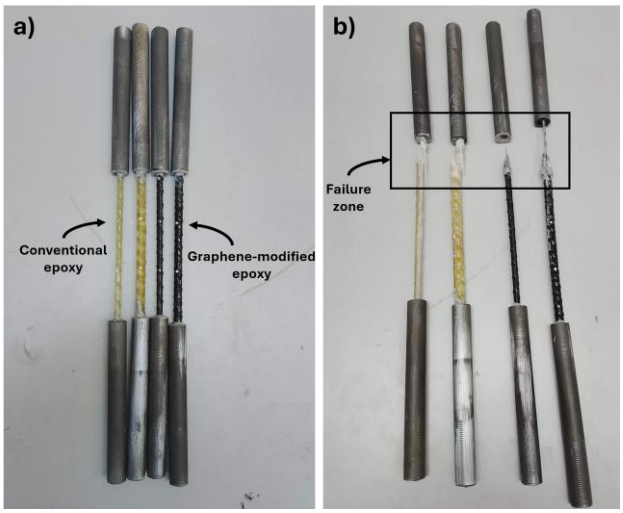


Figure 10: Tensile samples a) Before test b) After test

Figure 10 shows the tensile test specimen before and after test. Evidence of the brittle failure can be observed in the failed zone. Before testing, the GFRP bars were anchored at both ends using steel tubes as discussed in Section 3.1.1, leaving a centrally exposed region (gauge length) for tensile loading as shown in Figure 5. After testing, the fracture occurred within this exposed GFRP region near the anchorage, while the steel anchorage remained undamaged. The localized fracture and separation of the reinforcing fibers are consistent with the abrupt stress drop observed in Figure 8. Importantly, the absence

of the pre-mature anchorage failure indicates that the applied load was effectively transferred to the GFRP bars and that the measured failure was primarily associated with the reinforcement itself rather than failure of the gripping system.

In general, the study showed that the diameter of the bar had a positive influence on tensile strength and stiffness, while the graphene content decreased these two parameters compared to the traditional or conventional epoxy matrix. Nevertheless, the relatively small differences in tensile strain indicate that the modification had a less pronounced influence on the deformation capacity. The tensile properties indicate that the graphene-modified matrix does not necessarily improve tensile performance and its effect may depend strongly on the specific mechanical property being evaluated while further deep study and some tests like Fourier-Transform Infrared Spectroscopy (FTIR), Scanning Electron Microscopy (SEM) etc. needed to find the real reason for this decrease in the tensile strength.

4.1.2. Transverse Shear Strength (TSS) test

Shear properties were determined for the GFRP bars in order to study the effect of epoxy matrix modification with graphene as well as the diameter of the bar on the transverse resistance of the reinforcement. Fig. 11 shows the graphs of transverse shear strength-displacement relationships for the conventional epoxy (CE) and graphene-reinforced epoxy (GE) with diameters of 6, 8, and 12 mm. Table 6 summarizes the mean maximum TSS strength, coefficient of variance (CoV), and displacement at maximum TSS strength.

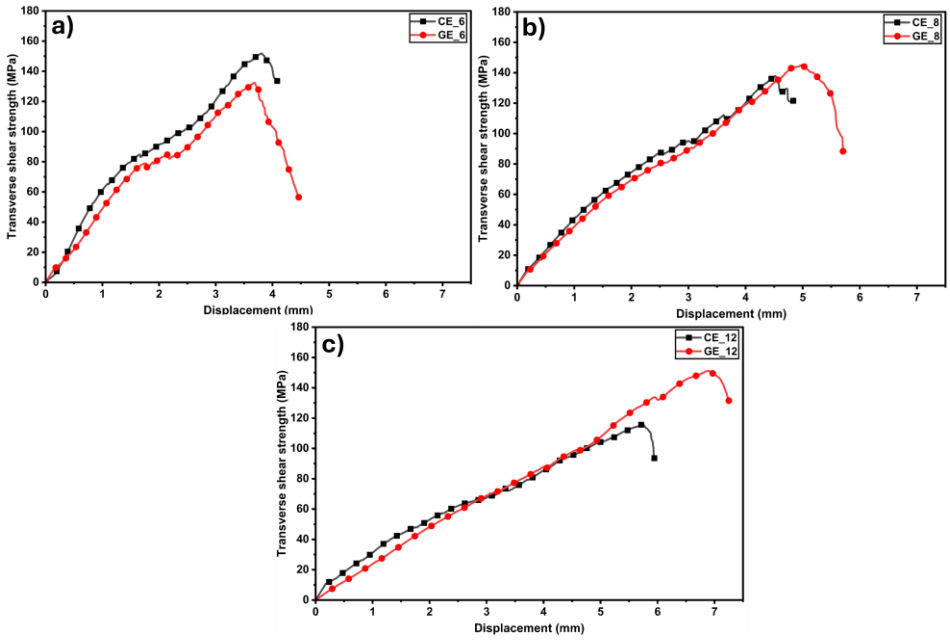


Figure 11: TSS test curve for a) 6 mm b) 8 mm and c) 12 mm diameter GFRP rebars

Table 6: Results summary of TSS test.

Series	Max. TSS		Displacement at max. TSS (mm)
	Mean (MPa)	CoV (%)	
CE_6	151.8	5.51	3.8
GE_6	132.3	11.21	3.7
CE_8	137.8	4.80	4.5
GE_8	145.2	7.02	5.0
CE_12	115.7	6.13	5.7
GE_12	151.2	10.31	6.9

The TSS curves (Figure 11) show a generally increasing response with displacement up to the maximum strength, followed by a reduction in strength associated with transverse shear failure. However, the shape of the curves differs noticeably with bar diameter and epoxy type. In Figure 11a, the 6 mm bars, the conventional epoxy specimen reached the highest strength of 151.8 MPa at 3.8 mm displacement, whereas the graphene-modified specimen reached 132.3 MPa at 3.7 mm. Thus, graphene modification resulted in a reduction of approximately 12.8% in the maximum TSS strength for the 6 mm bars. The relatively similar displacement at maximum strength indicates that the modification affected the load-carrying capacity more strongly than the displacement required to reach the peak.

However, when 8 mm bars were taken into consideration, a different trend was observed. The maximum strength of the TSS was found to increase from 137.8 MPa of CE_8 to 145.2 MPa of GE_8, representing an improvement of about 5.4% using graphene-modified epoxy system. Moreover, the displacement at maximum strength was found to be 4.5 mm for CE_8 but 5.0 mm for GE_8. This indicates that, unlike the 6 mm bars, graphene-reinforced 8 mm GFRP bars could bear a slightly higher transverse shear stress over a larger displacement at maximum strength. The graph of Figure 11b clearly depicts that GE_8 had a high load value close to its peak and showed a gradual response prior to failure.

There was also a much more noticeable impact of graphene modification seen with the bars of 12 mm in diameter as shown in Figure 11c. The conventional epoxy specimen demonstrated maximum TSS strength at only 5.7 mm, equal to 115.7 MPa, while the modified matrix one had the maximum TSS strength of 151.2 MPa at 6.9 mm, which means that there was an increase in maximum TSS strength of about 30.6%. The GE_12 curve continued to rise over a wider range of displacement than the CE_12 curve, which proves increased resistance to transverse deformation before attaining its maximum strength.

The TSS results obtained for the 12 mm bars can also be compared with those reported by Nepomuceno [3] for Ø12 Schöck GFRP rebars. For the unconditioned reference specimens, an average TSS of

166.2 MPa was reported. In the present study, CE_12 and GE_12 exhibited average TSS values of 115.7 MPa and 151.2 MPa, respectively, corresponding to values approximately 30.4% and 9.0% lower than the Schöck reference. Therefore, although the graphene-modified bar did not reach the TSS of the commercial Schöck rebar, the GE_12 result was considerably closer to this reference value than that obtained for CE_12. This comparison supports the observed improvement associated with graphene modification for the 12 mm configuration.

Nevertheless, the comparison should be interpreted as a benchmark rather than as a direct assessment of material performance. The Schöck bars investigated by Nepomuceno [3] consisted of a pultruded GFRP system with a vinyl-ester matrix and approximately 88% glass fiber by weight, whereas the bars investigated in the present work were produced with conventional or graphene-modified epoxy matrices. Similar to the tensile properties, described in the previous sub-section, differences in matrix composition, fiber content, manufacturing conditions and fiber–matrix interface may therefore contribute to the differences in TSS. Since transverse shear behavior is particularly dependent on the polymer matrix and fiber–matrix interface, these material differences are especially relevant when interpreting the results.

From the analysis of the results, it is clear that the effect of graphene on the composite material varied from one diameter of the bars to another. A decrease was noted for the 6 mm diameter bars, whereas there were slight and significant increases for the other two diameters, 8 mm and 12 mm. Such diameter-based variation implies that the interaction of the modified polymeric matrix with the reinforcing material used in the GFRP can be affected by the shape of the specimen and the resultant stress distribution upon transverse loading. Transverse shear strength is highly dependent on the matrix and fiber-matrix interface, and hence modifications of the matrix due to graphene could affect the redistribution of transverse stresses in the composite.

The effect of bar diameter on the influence can also be seen through comparison of the conventional epoxy series. The highest TSS strength dropped from 151.8 MPa for CE_6 to 137.8 MPa for CE_8 and 115.7 MPa for CE_12. It is evident that increasing diameter has not resulted in an equally increased shear strength. This is because TSS is a measure of stress and not total load; therefore, increasing diameter will not necessarily increase shear strength in the calculation. In contrast, the effect of graphene modification resulted in increased values in the TSS strengths from 132.3, 145.2, and 151.2 MPa for GE_6, GE_8, and GE_12 respectively. It can be suggested that with increasing bar diameter, the modified epoxy becomes relatively more efficient in resisting transverse shear strength.

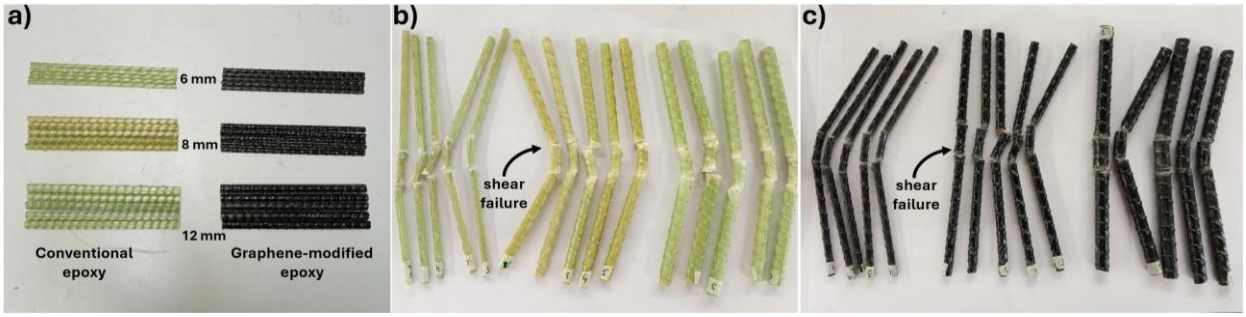


Figure 12: a) Prepared TSS samples before testing, b) and c) tested samples of conventional and graphene-modified epoxy respectively

The failure photos (Figure 12b and Figure 12c) give a clear physical link to the mechanical behavior. As illustrated in Figure 11b and c, the tested samples exhibited a clear localized shear failure area at the point of loading. The deformation occurs at the point where the transverse loading is applied, with a definite alteration in the bar's shape and clear damage to the composite material. This localized damage is in agreement with the gradual increase in TSS in the curves and the subsequent drop after the peak. The existence of the localized shear failure area in all the tested samples is an indication that the failure process was dominated by the transverse shear loading conditions.

4.1.3. Comparative analysis of mechanical performance

The combined analysis of the tensile and transverse shear results demonstrates that the influence of graphene modification was strongly dependent on the mechanical property considered. Under longitudinal tensile loading, graphene modification resulted in reductions in both tensile strength and elastic modulus for the 6 mm and 8 mm rebars. In contrast, the transverse shear response showed a diameter-dependent trend: the TSS decreased by approximately 12.8% for the 6 mm bars, increased slightly by approximately 5.4% for the 8 mm bars, and increased significantly by approximately 30.6% for the 12 mm bars. These different trends are consistent with the distinct mechanisms governing the two loading conditions. Tensile behavior is predominantly controlled by the longitudinal glass fibers and the efficiency of load transfer along the fiber direction, whereas transverse shear behavior is considerably more dependent on the polymer matrix and the fiber–matrix interface.

Among the TSS specimens, CE_6 exhibited the highest absolute transverse shear strength, reaching 151.8 MPa. However, GE_12 presented the highest TSS among the graphene-modified series, with 151.2 MPa, together with the largest displacement at maximum TSS. Furthermore, this value was only approximately 9% lower than the 166.2 MPa reported by Nepomuceno [3] for unconditioned Ø12 Schöck GFRP rebars. This comparison is particularly relevant because it indicates that, although the graphene-

modified Ø12 bar did not reach the TSS of the commercial Schöck reference, its transverse shear performance approached the same order of magnitude. Nevertheless, the comparison should be considered only as a benchmark, since the two GFRP systems differ in matrix composition, fiber content and manufacturing characteristics.

The graphene-modified series also consistently presented higher coefficients of variation than the corresponding conventional epoxy series, indicating greater scatter in the experimental response. The statistical analysis further indicated a significant effect of graphene modification for the 12 mm bars, although the overall effect of graphene considering all diameters was not statistically significant. Therefore, the present results do not support a general conclusion that graphene modification improves the mechanical performance of GFRP rebars. Instead, they suggest that its effectiveness is property- and geometry-dependent. In the present experimental conditions, graphene modification did not improve the longitudinal tensile response but showed clear potential to enhance matrix-dominated transverse shear behavior, particularly for the 12 mm rebars.

4.2. Concrete bond performance

The direct pull-out tests were performed to evaluate the bond behavior between the GFRP bars and concrete and to investigate the effects of bonded length and epoxy modification. The tested configurations comprised conventional epoxy (CE) and graphene-modified epoxy (GE) GFRP bars with bonded lengths of 5Ø and 10Ø, together with the Schock specimen (S_5Ø) used as a benchmark. Figure 12 presents the pull-out force–loaded-end slip and bond stress–slip curves, while the principal experimental results are summarized in Table 7.

The main parameters used to characterize the bond response were the maximum pull-out force (F_{max}), maximum bond strength (τ_{max}), slip corresponding to the maximum pull-out force, normalized bond strength (τ_{n}), and fracture energy (G_F). The maximum pull-out force was obtained directly from the experimental force–slip curves. The average bond strength was then calculated by relating this force to the nominal bonded surface area:

$$\tau_{max} = \frac{F_{max}}{\pi \emptyset L_b} \tag{4.1}$$

Where $\emptyset$ is the nominal bar diameter, and L_b is the bonded length. In the present study, corresponds to 5Ø or 10Ø.

To find the real loaded-end displacement S_l, the elastic deformation of GFRP bar must be subtracted from the LDVTs displacements using the equation:

$$s_l = \delta_{LVDTs} - \frac{FL_c}{E_f A_b} \tag{4.2}$$

Where δ_{LVDTs} is the loaded end displacement, F is the pull-out force, L_c is the distance between the loaded section and the location where the LVDT attachment clip is fixed to the rebar as shown in Fig. 8 (a).

To account for the influence of concrete strength when comparing the bond results, the bond strength was also normalized using the mean concrete compressive strength (f_{cm}) which is calculated as 25.1 MPa as mentioned in section 3.2.

The normalized bond strength was calculated using the equation:

$$\tau_n = \frac{\tau_{max}}{\sqrt{\frac{f_{cm}}{1MPa}}} \tag{4.3}$$

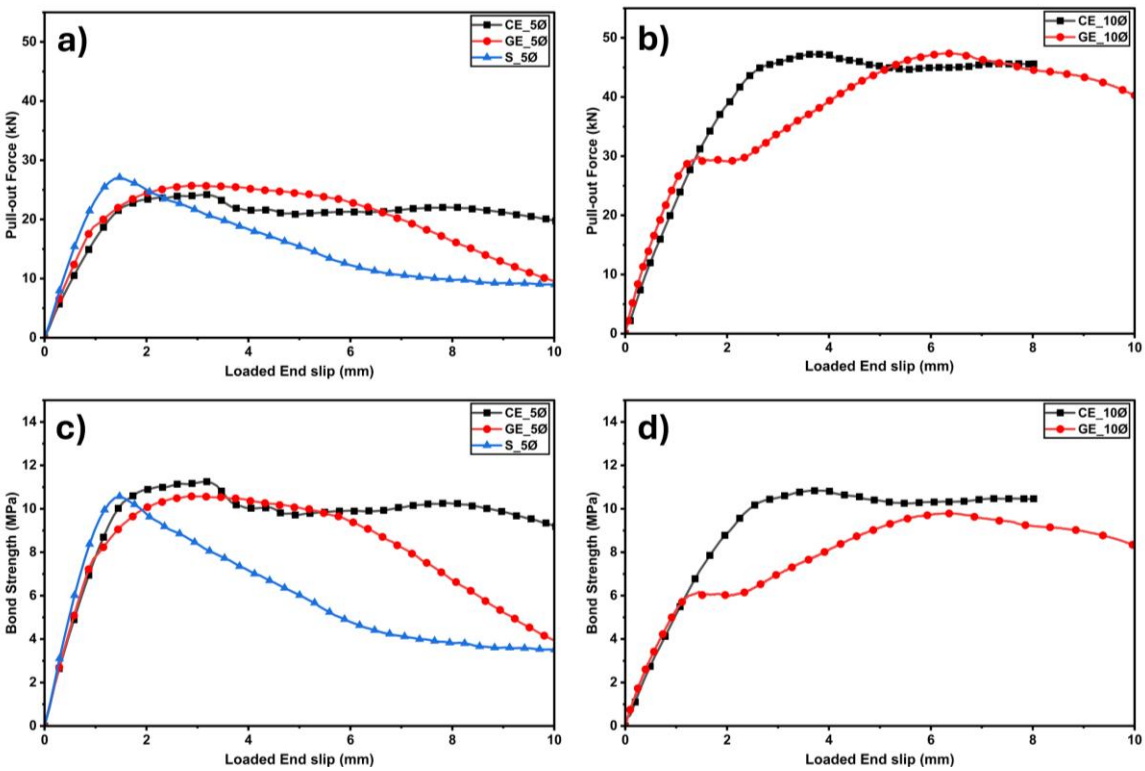


Figure 13: Pull-out test results a) Pull-out force vs slip and b) Bond strength vs slip

Table 7: Result summary of the direct pull-out test

Series	F_{max} (kN)	τ_{max} (MPa)	G_f kN.mm	τ_n (MPa)	S_{lmax} (mm)
CE_5Ø	24.1	11.2	204.82	2.23	3.2
GE_5Ø	25.6	10.6	197.40	2.11	2.9
S_5Ø	27.0	10.5	152.46	2.10	1.5
CE_10Ø	47.2	10.8	315.76	2.15	3.8
GE_10Ø	47.4	9.8	377.34	1.95	6.3

4.2.1. The Effect of bonded length and epoxy modification

For the 5Ø bonded length, CE_5Ø reached a maximum pull-out force of 24.1 kN, corresponding to a bond strength of 11.2 MPa at a loaded-end slip of 3.2 mm. GE_5Ø exhibited a slightly higher maximum pull-out force of 25.6 kN, but its bond strength was lower at 10.6 MPa, with the maximum force reached at 2.9 mm slip. Therefore, although the graphene-modified specimen sustained approximately 6.2% higher maximum pull-out force, this increase did not translate into a higher average bond strength. In normalized terms, the bond strength decreased from 2.236 for CE_5Ø to 2.116 for GE_5Ø. This indicates that the graphene modification did not significantly enhance the average interfacial bond resistance for the shorter bonded length under the present experimental conditions.

The schock benchmark, S_5Ø, reached the highest maximum pull-out force among the 5Ø specimens, with 27.0 kN, while its bond strength was 10.5 MPa and normalized bond strength was 2.096 which is consistent (on avaerge) what Nepomuceno [3] observed for schock rebar. Even though the maximum force of S_5Ø was about 12% greater than that of CE_5Ø, the normalized bond strength of S_5Ø was slightly less. The difference became even more evident in the case of slip at maximum force, as S_5Ø attained maximum bond strength at 1.5 mm, while it was 3.2 mm for CE_5Ø and 2.9 mm for GE_5Ø. It is clear from here that schock rebar attained maximum bond strength at much lesser deformation, but the GFRP rebars were more progressive in their load transfer mechanism but having more ductility.

he increase in the bonded length from 5Ø to 10Ø has resulted in a large increase in the total pull-out force. For the conventional epoxy system, the force increased from 24.1 kN for CE_5Ø to 47.2 kN for CE_10Ø, an increase of approximately 96%. Likewise, for the graphene-epoxy system, the force increased from 25.6 kN for GE_5Ø to 47.4 kN for GE_10Ø, which is an increase of about 85%. This large increase highlights the significance of the bonded length embedded in concrete.

Nevertheless, the increase in the maximum pull-out force was not matched with any increase in average bond strength. In fact, CE showed a slight decrease in bond strength from 11.2 MPa at 5Ø to 10.8 MPa at 10Ø, while GE showed a decrease in bond strength from 10.6 to 9.8 MPa. Normalized bond strengths also followed the same pattern, decreasing from 2.23 to 2.15 for CE and from 2.11 to 1.95 for GE. Such behavior shows that an increase in the bonded length increases the total interface area for transferring loads, but the increase in bonded length does not have an even effect on the average bond stress.

This may be attributed to the fact that the stress distribution along the length of the bonded section is not uniform. The area near the loaded end experiences higher stress levels at the interface, whereas lower levels of stress are transferred further down along the bonded section. With increasing bonded length, the extra interface thus contributes to the pullout force, yet it does not experience the same stress level as that of the highly stressed area near the loaded end..

4.2.2. Force–slip response and bond mechanisms

From Figure 12, the current set of tests does not follow the typical pattern of response of only one phase of the pull-out process. Instead, CE_10Ø and GE_10Ø demonstrate a more gradual progression in the development of resistance, with variations in slope and periods of stability or increase in load before the peak force is achieved. The pattern is quite different from a typical pull-out response in which there is an increase of force to a peak and continuous decrease after the peak.

Such response is a result of a gradual activation of the bond interface. When load is initially applied, the bond force is caused by the adhesion of the reinforcement to the surrounding concrete. As the slip is increased, the bond interface is damaged, causing adhesion to become less significant. Interlocking action by the ribs and friction between the surface ribs and concrete play a bigger role. Since these two factors may not occur in tandem for the whole bonded length, the force can still increase even when damage starts to occur.

The model thus explains why the 5Ø and 10Ø samples show different shapes of their respective curves. The longer bonded zone of the 10Ø sample gives more room for the development of the stress redistribution process. Damage may therefore be initiated in one area, but the remaining areas of the interface would still be transferring the loads. This interaction between the damaged and undamaged parts of the interface will then give rise to the plateau and secondary hardening behavior of the curves.

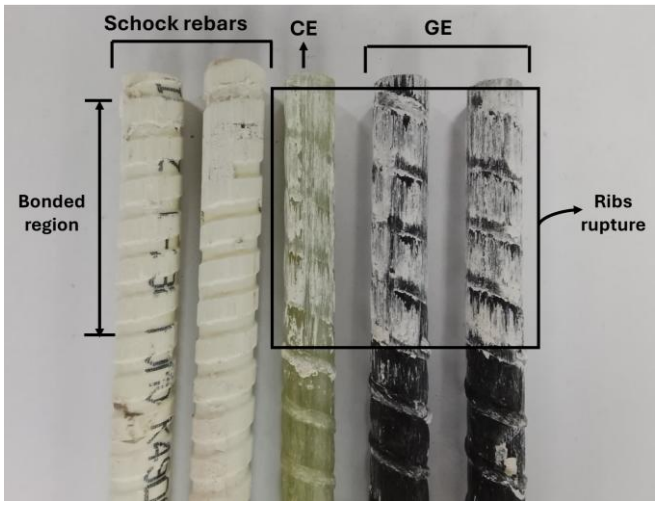


Figure 14: Failure mode of direct pull-out test

4.2.3. Failure observations

The post-test photos confirm the mechanisms that were behind the response. As can be seen from Figure 13, there is considerable damage to the ribs on the surface within the bonded area. Several ribs from the bonded area appear to have been sheared off and broken away. This confirms that the mechanism of failure was not limited to separation of the concrete and GFRP interface alone. The ribs themselves helped in providing mechanical interlocking, which then got damaged as the displacement progressed.

The rib detachment becomes particularly important when considering the load-carrying capacity after the maximum pull-out load. Once the initial contribution from the adhesive has been stripped away, the rest of the load can be carried by friction and mechanical interaction between the rib geometry and the surrounding concrete. This explains the progressive drop in force seen in many curves. A different failure appearance was observed for the Schöck rebar. In contrast to the CE and GE rebars, no evident rupture or detachment of the Schöck surface ribs was observed after testing. Instead, concrete remnants appeared to remain attached between and around the intact ribs. A similar pull-out failure mode was reported by Nepomuceno et al [3]., where concrete remained attached to intact GFRP ribs after testing. This distinction is particularly relevant because the same concrete was used for all rebar configurations in the present experimental campaign. Therefore, the different post-test failure appearances are more likely related to differences in the surface geometry, matrix characteristics, and mechanical resistance of the GFRP rebars. While the CE and GE specimens exhibited pull-out accompanied by significant rib damage, the Schöck specimen showed a pull-out mechanism with intact ribs, indicating a different local failure mechanism at the GFRP–concrete interface.

4.2.4. Fracture energy

The fracture energy (G_f) was used to characterize the energy dissipated during the debonding and pull-out process. It was determined from the area under the pull-out force versus loaded-end slip curve:

$$G_f = \int_0^{s_{max}} F(s)\, ds \tag{4.4}$$

Where F represents the pull-out force as a function of loaded-end slip and is the selected maximum slip. In this study, the integration was performed up to 10 mm slip. The results shown in table 7. The CE_10Ø dataset available for integration terminated at approximately 8.02 mm; therefore, its calculated value of 315.76 kN·mm represents the area up to the available experimental slip rather than a complete 0–10 mm integration.

The fracture-energy results provide an additional perspective that cannot be obtained from maximum bond strength alone. Although GE_5Ø had a slightly higher maximum pull-out force than CE_5Ø, its fracture energy was slightly lower. This indicates that the ultimate force and the overall energy dissipated during pull-out are not necessarily governed by the same mechanisms. In contrast, the substantially higher energy associated with GE_10Ø is consistent with its extended force–slip response and the larger displacement required to reach maximum pull-out force. Only one specimen was tested for the GE_10Ø configuration, as the second specimen failed during testing. Therefore, the corresponding force–slip curve represents a single-specimen response. Consequently, the observed increase in bond performance cannot be considered conclusive, even though the improvement was not statistically significant.

4.2.5. Comparison of CE and GE systems

The results indicate that the effect of graphene modification cannot be described simply as either beneficial or detrimental to bond performance. For the 5Ø configuration, GE exhibited a slightly higher pull-out force but lower bond strength and fractured energy than CE. For the 10Ø configuration, the maximum pull-out forces of CE and GE were almost identical, while GE exhibited a lower bond strength but a substantially more extended force–slip response.

The reduction in normalized bond strength from CE to GE at both bonded lengths suggests that the graphene modification did not increase the average interfacial bond stress under the present conditions. However, the different curve shapes and the higher displacement associated with GE_10Ø indicate that the modification may have altered the way damage developed and propagated along the interface.

Changes in matrix properties, fiber–matrix interaction, and the local mechanical interaction between the modified GFRP surface and concrete may contribute to this behavior. Nevertheless, these mechanisms should be regarded as possible explanations rather than definitive conclusions without dedicated microstructural or interface-level characterization.

Overall from the direct pull-out tests, it is clear that the effect of bonded length on the maximum pull-out force is far greater than the effect of bond strength. The increase in bonded length from 5Ø to 10Ø almost doubled the maximum pull-out force, but the average bond strength reduced slightly. Thus, it is evident that the increase in the embedded length increases the total anchorage capacity without increasing the average interfacial stress capacity.

The modified epoxy showed less normalized bond strength than the conventional epoxy, but the effect of the graphene-modified epoxy on the force-slip behavior was more complicated. The progressive curve behavior, increased slip at peak force of GE_10Ø, and rib shearing show that the bond behavior was controlled by the joint effect of adhesion, friction, interlocking, progressive rib damage, and stress transfer along the bonded length. Therefore, evaluating the bond performance solely from maximum pull-out force or bond strength would not fully capture the differences between the two epoxy systems. The inclusion of normalized bond strength and fractured energy provides a more comprehensive assessment of interfacial behavior.

5. PARAMETRIC STUDY

5.1. Analytical method for bond test

To further investigate the bond behavior between the reinforcing bars and concrete, an analytical modelling procedure was adopted based on the local bond stress–slip ($\tau - s$) relationship. The analytical representation of the pull-out phenomenon can be established from the equilibrium of an infinitesimal element of the embedded reinforcing bar. In the present formulation, the bond behavior is described in terms of slip, and the local bond law is obtained through an inverse analysis procedure, in which the analytical pull-out response is iteratively adjusted to reproduce the experimental pull-out force–loaded-end slip response. This approach has previously been applied successfully to different types of bonded reinforcement and pull-out configurations [59]

Consider an infinitesimal element of the reinforcing bar embedded in concrete. Equilibrium of this element gives the relationship between the axial force in the bar and the interfacial bond stress:

$$\sigma_f A_f \; + \; \tau \, P_f \, dx \; = \; \left(\sigma_f + \; d\sigma_f\right) A_f \tag{5.1}$$

Where σ_f is the axial stress in the reinforcing bar, A_f is its cross-sectional area, τ is the local bond shear stress and P_f is the perimeter of the reinforcing bar. Assuming linear-elastic behaviour of the reinforcing bar, $d\sigma_f = E_f \, d\varepsilon_f$ and neglecting the deformation of the surrounding concrete in the evaluation of slip, the governing differential equation can be expressed as:

$$\frac{d^2 s}{dx^2} = \frac{P_f}{E_f A_f} \tau(s) \tag{5.2}$$

Where s the local slip is between the reinforcing bar and the surrounding concrete, E_f is the longitudinal elastic modulus of the reinforcing bar, A_f is its cross-sectional area and P_f is its perimeter.

The above equation demonstrates that the distribution of slip along the anchorage length is directly governed by the local bond stress acting at the bar–concrete interface. Therefore, once an appropriate $\tau - s$ relationship is defined, the local slip distribution and consequently the global pull-out force–slip response can be obtained.

5.1.1. Local bond stress–slip relationship

In this study, the local bond law was represented by a two-branch relationship consisting of an ascending pre-peak branch and a descending post-peak branch:

$$\tau(s) = \begin{cases} \tau_m \left(\frac{s}{s_m}\right)^{\alpha}, & s \leq s_m \\ \tau_m \left(\frac{s}{s_m}\right)^{\acute{\alpha}}, & s > s_m \end{cases} \quad (5.3)$$

where:

- $\tau(s)$ = local bond shear stress at a given slip s
- τ_m = maximum local bond stress
- s_m = slip corresponding to the maximum local bond stress
- α = parameter controlling the shape of the pre-peak/ascending branch
- $\acute{\alpha}$ = parameter controlling the shape of the post-peak/descending branch

The global pull-out force is then obtained by integrating the local bond response along the anchorage length. In the adopted formulation, the pull-out force is expressed as:

$$N = \sqrt{2\, E_f A_f P_f \int_{s_f}^{s(x=L_b)} \tau(s) ds} \quad (5.4)$$

Where L_b is the anchorage length, s_f and $s(x = L_b)$ represent the relevant slip conditions along the bonded length. The formulation therefore establishes a direct connection between the local $\tau - s$ relationship and the experimentally measurable global pull-out force–slip response.

5.1.2. Inverse analysis procedure

The parameters defining the local bond stress–slip relationship, namely τ_m, s_m, α and α', cannot be obtained directly from the experimentally measured global pull-out force–loaded-end slip response. Therefore, these parameters were identified through an inverse analysis procedure in which the local bond law was iteratively calibrated until the corresponding analytical response provided the best possible agreement with the experimental curve.

The numerical procedure adopted in the present study follows the Genetic Algorithm (GA)-based inverse identification methodology previously applied by Correia et al. [60] for the identification of local FRP–concrete bond laws. The underlying analytical formulation follows the inverse-analysis approach originally developed by J. Sena-Cruz [59]. For each candidate combination of τ_m, s_m, α and α', the governing differential equation presented in Eq. (5.2) was numerically solved along the bonded length, considering the corresponding boundary conditions. This solution provides the slip and bond-stress distributions along the bonded length and, consequently, the corresponding global pull-out force–loaded-end slip response.

A Genetic Algorithm was used to identify the optimum combination of the four bond-law parameters. The GA was implemented using a population of 40 individuals and a maximum of 100 generations. Genetic recombination was performed using a crossover rate of 0.8, while population diversity was maintained using a mutation rate of 0.3. Mutation was introduced through a Gaussian perturbation with a standard deviation corresponding to 15% of the admissible range of each parameter. A stagnation criterion of 10 generations was also adopted. When no improvement in the objective function was obtained during 10 consecutive generations, the optimization was restarted to promote further exploration of the parameter space and reduce the possibility of convergence towards a local minimum.

Following the procedure adopted by Correia et al. [60], the peak-slip parameter s_m, was searched between 0.01 and 1.50 mm, the maximum local bond stress τ_m between 5.0 and 40.0 MPa, and the shape parameters α and α' between 0.1 and 1.0. The longitudinal elastic modulus of the GFRP reinforcement, obtained experimentally from the mechanical characterization presented in Section 4.1, was introduced directly into the analytical model and was therefore not considered an optimization variable. The geometrical parameters, including the GFRP cross-sectional area, perimeter and bonded length, were defined individually for each tested configuration.

To improve the efficiency of the optimization, a hybrid initialization procedure was adopted for the first generation. Half of the initial population was generated randomly within the prescribed parameter ranges, while the remaining 50% was initialized using a physically informed estimate of the peak bond stress. This initial estimate was obtained from the experimentally measured maximum pull-out force and the bonded surface area according to: $\tau_{max} = \frac{F_{max}}{p_f L_b}$ where F_{max} is the experimental maximum pull-out force, m$p_f$is the effective perimeter of the GFRP rebar and L_b is the bonded length. This procedure provides the GA with initial candidate solutions located closer to physically meaningful regions of the search space while maintaining sufficient population diversity.

For each candidate parameter set, the numerical pull-out force–loaded-end slip curve was compared with the corresponding experimental response. The primary objective of the optimization was to minimize the area-based error, e, between the experimental and analytical curves. In addition, the differences between the experimental and numerical maximum pull-out force and the corresponding loaded-end slip were considered in the fitness evaluation. In the methodology adopted by Correia et al.[60], candidate solutions were considered feasible when the errors associated with the maximum pull-out force (eforce) and the slip at maximum force (eslip) were lower than 2%, with an additional weighted contribution of these peak errors used to refine the selection of the optimum solution.

Through the successive processes of evaluation, selection, crossover and mutation, the population evolved towards parameter combinations producing progressively closer agreement between the numerical and experimental responses. The final values of τ_m, s_m, α and α' correspond to the optimum solution identified by the GA for each individual pull-out specimen.

The inverse identification constitutes a nonlinear optimization problem and does not necessarily lead to a unique set of local bond-law parameters. Different combinations of parameters may potentially reproduce similar global pull-out responses. Therefore, the identified values should be interpreted as calibrated effective parameters of the adopted bond stress–slip law rather than as unique material constants. This procedure is particularly useful because the experimentally accessible quantity is the global pull-out force–loaded-end slip relationship, whereas numerical bond modelling requires a local bond stress–slip relationship. The inverse analysis therefore provides a means of translating the experimentally measured global response into a representative local constitutive law describing stress transfer along the bonded length.

5.1.3. Comparison between experimental and analytical responses

Figure 15 presents the comparison between the experimental and analytically predicted pull-out force–loaded-end slip curves for the investigated reinforcing bars. The analytical curves were generated using the calibrated local bond stress–slip parameters described above. The comparison allows the ability of the adopted local bond law to reproduce the experimental response to be evaluated for the different bar types and anchorage configurations. Tables 8 are the summarized results and the parameter used in this parametric study. Same nomenclature is adopted as used in materials characterization and bond performance. Here S1 and S2 represent sample 1 and sample 2, as previously mentioned that two samples were for each series except GE_10 one sample failed so the plotted and table data is only for one sample in this specific case.

5.1.4. Schock reference bars

For S1–S_5Ø, Figure 15(a), the experimental response increases almost linearly at the beginning of loading and reaches a maximum pull-out force of approximately 28 kN at a slip of about 1.5 mm. The analytical curve reproduces the initial ascending response and reaches a very similar maximum force. The corresponding parameters (shown in table 8) obtained from the inverse analysis are s_m= 1.50 mm, τ_m = 13.2 MPa, α = 0.84 and $\acute{\alpha}$ = 0.14. The relatively good agreement around the peak indicates that the adopted local bond law is capable of representing the dominant bond-transfer mechanism for this specimen.

For S2–S_5Ø, Figure 15(b), the experimental maximum force is approximately 20.2 kN, occurring at a slip of approximately 1.5 mm. Again, the analytical response reproduces the ascending branch and the vicinity of the maximum response reasonably well. However, differences become progressively more evident in the post-peak region, where the experimental response exhibits a more gradual reduction in load than the analytical curve.

5.1.5. Conventional epoxy GFRP bars

Regarding S1-CE_5Ø, shown in Figure 15(c), the experimental maximum pull-out force is about 28 kN, and the analytical curve gives a good approximation of both the increasing and the peak regions. Yet, following the maximum point, the experimental curve is fluctuating and presents a longer residual load-carrying region, whereas the analytical curve follows a smoother decreasing path.

Similar observations are made for S2-CE_5Ø in Figure 15(d). The analytical curve gives an estimate of the initial increase of the pull-out force and of the position of the maximum point. Yet, the experimental curve keeps a relatively higher residual load during the subsequent slip range, whereas the analytical one predicts a continued decrease in bond strength. The reason behind such a difference is that the real post-peak behavior of the bond involves progressive redistribution of stresses along the length of the anchor, whereas the proposed analytical method models it by a single branch.

5.1.6. Graphene-modified epoxy GFRP bars

Differences between experimental and analytical behavior become even more obvious for graphene-enhanced GFRP bars. As for S1-GE_5Ø, Figure 15(e), the experimental curve achieves an initial peak of about 20 kN, after which it decreases and then recovers up to about 23-24 kN. The analytical behavior

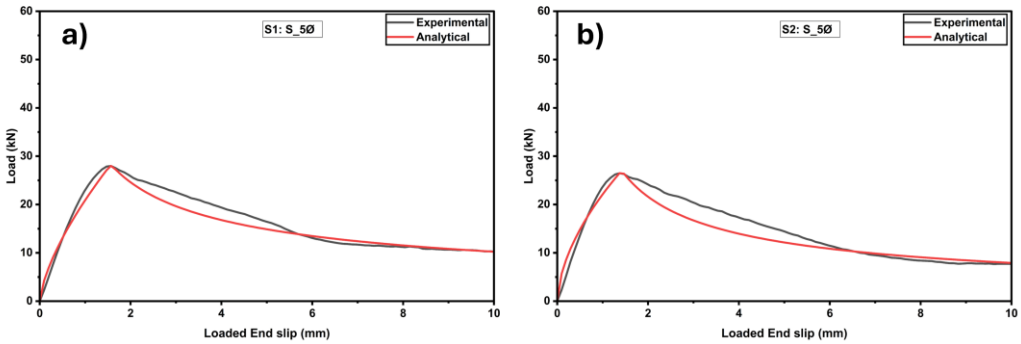
achieves about 24.2 kN at at s_m= 1.63 mm and then decreases. Therefore, while the analytical model gives a fairly good prediction of the general level of loads, it fails to capture the intermediate decrease and recovery seen in the experiments.

In the case of S2–GE_5Ø, Figure 15(f), analytical and experimental responses are clearly incompatible. After several optimization attempts, including runs in which the predefined parameter limits were relaxed, no satisfactory solution could be obtained. The best solution still presented errors greater than 70% for all three evaluation criteria: the area-based error, the error in the slip corresponding to the maximum force (e_{slmax}), and the error in the maximum pull-out force (e_{Fmax}). Therefore, the simulation results for this case are not considered because the significant difference between two curves shows that the two-branch local bond law used is not capable of reproducing the experimental response.

Regarding S1-CE_10Ø, Figure 15(g), the analytical solution shows that the peak pull-out force is about 45.1 kN, which is almost identical to the experimental peak of 45 kN. However, the analytical peak comes at smaller slip values and is then followed by a gradual decline, while the experimental response keeps increasing and even forms a second load-bearing zone at large slip values.

With regard to S2-CE_10Ø, Figure 15(h), there is excellent agreement concerning the peak pull-out capacity. The experimental response attains a value of about 50 kN, while the analytical solution gives a value of 50.7 kN. Nonetheless, the experimental response sustains a relatively high residual load for large slip values, unlike the analytical post-peak branch.

Finally, S1–GE_10Ø, Figure 15(i), exhibits one of the largest discrepancies. The experimental response continues to increase up to approximately 47 kN and maintains a high load level over a considerable slip range. In contrast, the analytical model reaches only approximately 31.6 kN before entering the descending branch. This result suggests that the adopted local bond law underestimates the sustained bond resistance of this particular graphene-modified GFRP configuration, the results are not sure in this case as only one specimen was tested, and one was failed during the test.



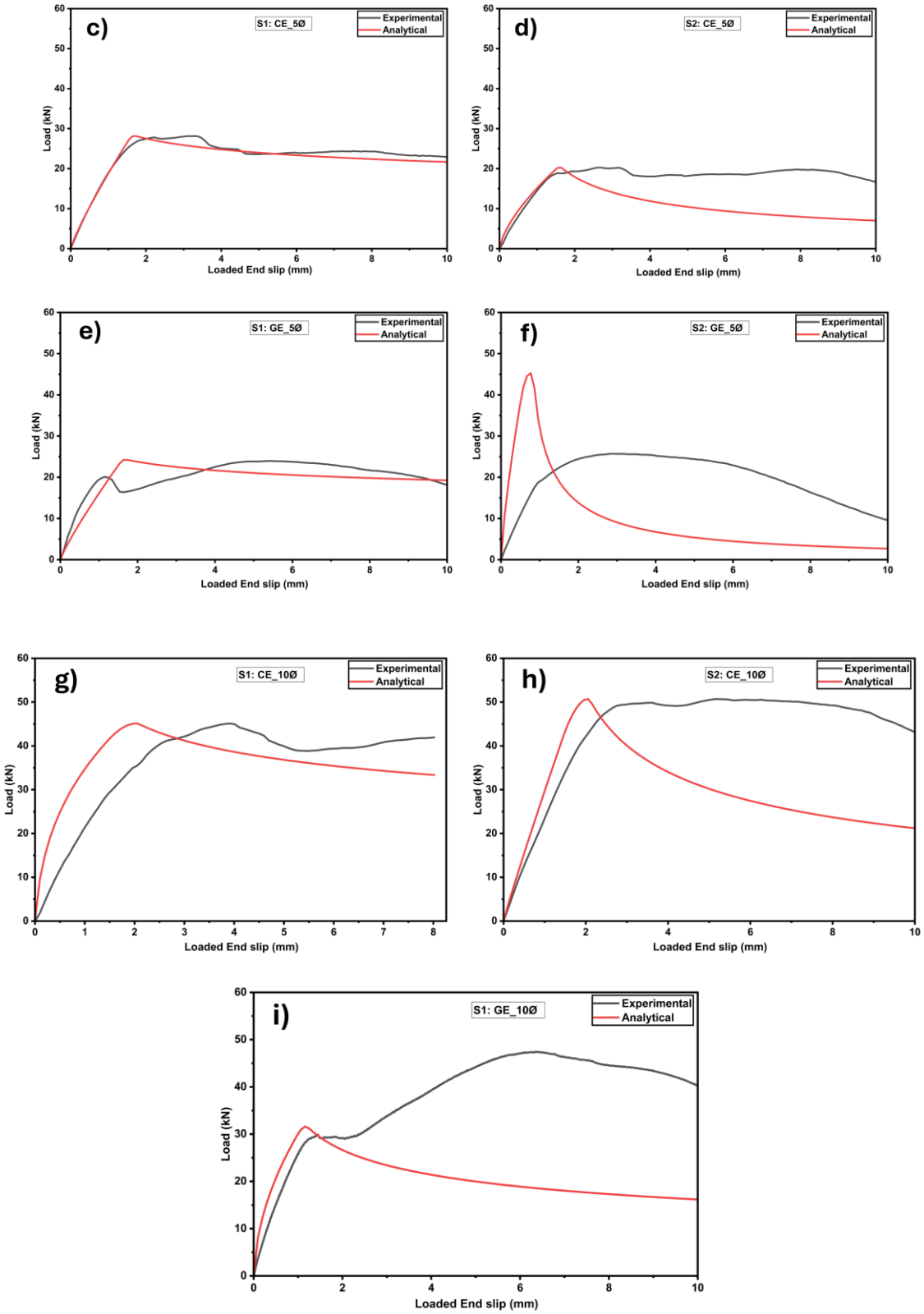


Figure 15: Comparison of experimental and analytical results of direct pull-out test a) and b) S_5Ø, c) and d) CE_5Ø, e) and f) GE_5Ø, g) and h) CE_10Ø and i) GE_10Ø

Table 8: Local bond stress-slip parameters resulted from analysis of the direct pull-out tests.

Sample	Series	S_{max} (mm)	F_{max} (kN)	τ_{max} (MPa)	α	α'	e_{area} (%)	e_{Slmax} (%)	e_{Fmax} (%)
S1	CE_5Ø	1.50	28.1	13.2	0.84	0.14	6.0	47.0	0.0
S2	CE_5Ø	1.54	20.2	9.4	2.1	0.18	15.8	39.2	0.0
S1	GE_5Ø	1.63	24.2	10.0	0.86	0.12	13.5	67.8	1.15
S1	S_5Ø	1.56	28.0	11.0	0.66	0.53	6.8	0.0	0.0
S2	S_5Ø	1.37	26.5	10.5	0.56	0.61	10.6	0.0	0.0
S1	CE_10Ø	2.05	45.1	10.6	0.37	0.19	18.2	47.4	0.0
S2	CE_10Ø	2.05	50.7	12.3	0.92	0.48	38.9	60.3	0.0
S1	GE_10Ø	1.15	31.63	12.0	0.50	0.62	17.1	63.6	2.0

* e_{area} = The area-based error between the experimental and analytical force–slip curves,
e_{Slmax} = The relative error in the maximum pull-out force
e_{Fmax} = The relative error in the loaded-end slip corresponding to the maximum pull-out force.

Overall, the inverse-analysis approach provides a useful representation of the initial bond mobilization and maximum pull-out capacity for several of the investigated specimens. This is consistent with the original analytical methodology, in which numerical force–slip responses were obtained from calibrated local $\tau - s$ laws and compared directly with experimental pull-out responses. The reference study reported that the same procedure could reproduce the principal characteristics of the experimental force–slip curves.

However, the present results also demonstrate an important limitation of the adopted formulation. The local bond law consists of only one ascending and one descending branch and therefore assumes a relatively smooth evolution of bond stress with slip. Several experimental curves, particularly those obtained for the graphene-modified GFRP bars, show multiple changes in slope, load drops, recovery of load and extended residual resistance. Such behavior cannot be fully captured by the adopted two-branch formulation.

This difference is particularly important for the specimens with 10Ø anchorage length, where a larger bonded interface is mobilized. Previous experimental work has shown that increasing the anchorage length increases the maximum pull-out force because a larger contact surface between the reinforcing bar and concrete becomes mobilized. Therefore, once local damage develops near the loaded end, the remaining portion of the anchorage can continue contributing to load transfer. The resulting progressive redistribution of bond stresses can produce the extended residual and plateau regions observed experimentally.

Accordingly, the analytical model should be regarded as a simplified representation of the overall bond mechanism rather than an exact reproduction of every local fluctuation in the experimental response. The calibrated parameters, s_m, τ_m, α and $\acute{\alpha}$ represent important quantitative indicators of the local bond characteristics, but the differences between the experimental and analytical curves show the necessity of using more sophisticated bond models in the case of progressive rib deterioration and bond redistribution along the bar length.

THIS PAGE WAS INTENTIONALLY LEFT BLANK

6. CONCLUSION, FUTURE WORK AND RECOMMENDATIONS

6.1.1. Conclusion

The main conclusions obtained from the experimental and analytical investigation can be summarized as follows:

- Modification of epoxy with graphene led to a property-specific effect instead of a general enhancement. The addition of graphene to the epoxy composite decreased longitudinal tensile strength and modulus in this case, but its impact on shear strength and adhesion was highly dependent on bar diameter and the mode of failure.
- The tensile properties were compromised by the addition of graphene. The tensile strength was reduced by 15.8% for 6mm bars and 16.2% for 8mm bars, whereas the tensile strain did not change much. An increase in the diameter from 6mm to 8mm enhanced the strength and elastic modulus of both epoxy systems.
- Transverse shear response was found to follow the reverse trend in the case of larger bars. Graphene decreased TSS of 6 mm by around 12.8%, while an increase of 5.4% and 30.6% was observed for 8 mm and 12 mm, respectively. This proves that the graphene reinforced matrix performs better under matrix and interface dominant transverse loads. Although the statistical analysis shows the overall effect of graphene modification is not significant.
- Bond length had a strong influence on pull-out capacity. Increasing the bonded length from 5Ø to 10Ø approximately doubled the maximum pull-out force for both CE and GE systems, while the average bond strength does not change significantly. This indicates that a longer bonded region increases the total load-transfer capacity but does not proportionally increase the average interfacial bond stress.
- Graphene did not provide a consistent improvement in bond strength. The GE specimens showed similar or slightly higher pull-out capacity in some cases, but their average bond strength was not higher than the CE specimens. Instead, graphene mainly influenced the shape and deformation capacity of the bond response, with some GE specimens exhibiting extended residual resistance and more pronounced post-peak behavior.
- Bond failure was governed by progressive interfacial damage, involving adhesion, friction, mechanical interlocking and, importantly, shearing/removal of the surface ribs of the GFRP bars.

The observed rib damage explains the irregular post-peak responses and indicates that bond degradation occurred progressively rather than through an instantaneous loss of capacity.

- The local bond-slip analysis successfully described the main response for several specimens, particularly the initial loading stage and maximum pull-out force. However, the adopted two-branch law could not fully reproduce secondary load development, residual resistance and complex post-peak behavior, especially for some graphene-modified specimens.
- Overall, the results demonstrate that graphene modification should be optimized for the specific performance requirement. Under the conditions investigated, it was more promising for transverse shear behavior of larger-diameter bars than for longitudinal tensile or average bond strength enhancement.

6.1.2. Future work and recommendations

- Prior characterization and verification of the fiber volume fraction in both conventional and graphene-modified GFRP systems are recommended to ensure that the comparison is conducted under equivalent material conditions and to distinguish the effect of graphene modification from variations in fiber content.
- Future experimental campaigns should follow the applicable ASTM standards without modification, particularly regarding specimen dimensions, and number of samples. This would improve the consistency, repeatability, and reliability of the experimental results and facilitate more robust comparisons between the investigated systems.
- Optimize graphene content and dispersion through systematic investigation of different graphene concentrations, dispersion conditions and manufacturing parameters to identify the optimum matrix formulation.
- Investigate the underlying mechanisms using Scanning electron microscopy (SEM), FTIR and other microstructural techniques to relate graphene dispersion, fiber–matrix adhesion and damage development to the measured mechanical properties.
- Enhance the bond experimental test program by testing more specimens and varying the bar diameters, bond lengths, concrete strengths, and confinement, especially for the GE_10Ø specimen.
- Conduct a more advanced and detailed study on the local bond-slip law through incorporation of rib breakage, stress transfer, and residual friction in order to simulate the several phases in the experimentally observed force–slip response.

7. REFERENCES

[1] Y. Zhang and D. Gao, "Tensile property analysis of carbon/glass hybrid fibers-reinforced graphene-modified polymer bars," *Constr. Build. Mater.*, vol. 403, Nov. 2023, doi: 10.1016/j.conbuildmat.2023.133178.

[2] K. Brózda, J. Selejdak, and P. Koteš, "Accepted 21. Mart 2017. Available 30," *Applied Engineering Letters*, vol. 2, no. 1, pp. 6–10, 2017.

[3] E. Nepomuceno, "Development of sustainable GFRP-reinforced seawater concrete", PhD Thesis, University of Minho (2025).

[4] Q. S. Khan, M. Neaz Sheikh, and M. N. S. Hadi, "TENSION AND COMPRESSION TESTING OF FIBRE REINFORCED POLYMER (FRP) BARS," 2015.

[5] H. Sepetcioglu *et al.*, "Improved mechanical properties of graphene-modified basalt fibre-epoxy composites," *Nanotechnol. Rev.*, vol. 13, no. 1, Jan. 2024, doi: 10.1515/ntrev-2024-0052.

[6] Y. Zhang, D. Gao, D. Fang, L. Yang, Y. Pang, and J. Tang, "Durability of graphene-modified epoxy vinyl resin served as matrix phase of composite bar in simulated concrete environment," *Journal of Building Engineering*, vol. 68, Jun. 2023, doi: 10.1016/j.jobe.2023.106106.

[7] S. N. A Azraai, K. S. Lim, N. Yahaya, and N. M. Noor, "Characterization of Mechanical Properties of Graphene-Modified Epoxy Resin for Pipeline Repair."

[8] "Test Method for Bond Strength of Fiber-Reinforced Polymer Matrix Composite Bars to Concrete by Pullout Testing," Feb. 01, 2020, *ASTM International, West Conshohocken, PA*. doi: 10.1520/D7913_D7913M-14R20.

[9] Y. Ren, H. Wang, Z. Guan, and K. Yang, "Evaluation of the properties and applications of FRP bars and anchors: A review," Jan. 01, 2023, *Walter de Gruyter GmbH*. doi: 10.1515/rams-2022-0287.

[10] I. S. Abbood, S. A. Odaa, K. F. Hasan, and M. A. Jasim, "Properties evaluation of fiber reinforced polymers and their constituent materials used in structures - A review," in *Materials Today: Proceedings*, Elsevier Ltd, 2021, pp. 1003–1008. doi: 10.1016/j.matpr.2020.07.636.

[11] "Design and construction of building structures with fibre-reinforced polymers."

[12] S. Kocaoz, V. A. Samaranayake, and A. Nanni, "Tensile characterization of glass FRP bars," *Compos. B Eng.*, vol. 36, no. 2, pp. 127–134, Mar. 2005, doi: 10.1016/j.compositesb.2004.05.004.

[13] A. Wiater and T. Siwowski, "Comparison of tensile properties of glass fibre reinforced polymer rebars by testing according to various standards," *Materials*, vol. 13, no. 18, Sep. 2020, doi: 10.3390/ma13184110.

[14] "Test Method for Tensile Properties of Fiber Reinforced Polymer Matrix Composite Bars," Mar. 15, 2006, *ASTM International, West Conshohocken, PA*. doi: 10.1520/D7205_D7205M-06.

[15] Y. J. You, J. H. J. Kim, S. J. Kim, and Y. H. Park, "Methods to enhance the guaranteed tensile strength of GFRP rebar to 900 MPa with general fiber volume fraction," *Constr. Build. Mater.*, vol. 75, pp. 54–62, Jan. 2015, doi: 10.1016/j.conbuildmat.2014.10.047.

[16] S. Stankovich *et al.*, "Graphene-based composite materials," *Nature*, vol. 442, no. 7100, pp. 282–286, Jul. 2006, doi: 10.1038/nature04969.

[17] J. Wei, T. Vo, and F. Inam, "Epoxy/graphene nanocomposites - processing and properties: a review," *RSC Adv.*, vol. 5, no. 90, pp. 73510–73524, Aug. 2015, doi: 10.1039/c5ra13897c.

[18] J. A. King, D. R. Klimek, I. Miskioglu, and G. M. Odegard, "Mechanical properties of graphene nanoplatelet/epoxy composites," *J. Appl. Polym. Sci.*, vol. 128, no. 6, pp. 4217–4223, Jun. 2013, doi: 10.1002/app.38645.

[19] F. Wang, L. T. Drzal, Y. Qin, and Z. Huang, "Mechanical properties and thermal conductivity of graphene nanoplatelet/epoxy composites," *J. Mater. Sci.*, vol. 50, no. 3, pp. 1082–1093, Feb. 2015, doi: 10.1007/s10853-014-8665-6.

[20] M. A. Rafiee, J. Rafiee, Z. Wang, H. Song, Z. Z. Yu, and N. Koratkar, "Enhanced mechanical properties of nanocomposites at low graphene content," *ACS Nano*, vol. 3, no. 12, pp. 3884–3890, Dec. 2009, doi: 10.1021/nn9010472.

[21] G. Mittal, V. Dhand, K. Y. Rhee, S. J. Park, and W. R. Lee, "A review on carbon nanotubes and graphene as fillers in reinforced polymer nanocomposites," Jan. 25, 2015, *Korean Society of Industrial Engineering Chemistry*. doi: 10.1016/j.jiec.2014.03.022.

[22] W. Qin, C. Chen, J. Zhou, and J. Meng, "Synergistic effects of graphene/carbon nanotubes hybrid coating on the interfacial and mechanical properties of fiber composites," *Materials*, vol. 13, no. 6, Mar. 2020, doi: 10.3390/ma13061457.

[23] T. Topkaya, Y. H. Çelik, and E. Kilickap, "Mechanical properties of fiber/graphene epoxy hybrid composites," *Journal of Mechanical Science and Technology*, vol. 34, no. 11, pp. 4589–4595, Nov. 2020, doi: 10.1007/s12206-020-1016-4.

[24] V. Kumar Dwivedi and D. Kumar, "Graphene as a stimulus for mechanical strength in glass-fiber reinforced polymers composite," *World Journal of Engineering*, vol. 20, no. 1, pp. 143–149, Jan. 2023, doi: 10.1108/WJE-02-2021-0110.

[25] V. G. S. Veerakumar, B. P. Shanmugavel, and S. Harish, "On the Influence of the Functionalization of Graphene Nanoplatelets and Glass Fiber on the Mechanical Properties of GFRP Composites," *Applied Composite Materials*, vol. 28, no. 4, pp. 1127–1152, Aug. 2021, doi: 10.1007/s10443-021-09908-9.

[26] S. Kumar, V. Mahesh, V. Mahesh, and D. K. HarurSampath, "Improving physical, mechanical and interfacial properties of glass fiber composites using modified resin system with amine-functionalized and silanized graphene nanoparticles," *Polym. Compos.*, vol. 46, no. 12, pp. 11526–11541, Aug. 2025, doi: 10.1002/pc.29701.

[27] S. N. A Azraai, K. S. Lim, N. Yahaya, and N. M. Noor, "Characterization of Mechanical Properties of Graphene-Modified Epoxy Resin for Pipeline Repair."

[28] Y. Zhang and D. Gao, "Tensile property analysis of carbon/glass hybrid fibers-reinforced graphene-modified polymer bars," *Constr. Build. Mater.*, vol. 403, Nov. 2023, doi: 10.1016/j.conbuildmat.2023.133178.

[29] S. Kocaoz, V. A. Samaranayake, and A. Nanni, "Tensile characterization of glass FRP bars," *Compos. B Eng.*, vol. 36, no. 2, pp. 127–134, Mar. 2005, doi: 10.1016/j.compositesb.2004.05.004.

[30] A. Wiater and T. Siwowski, "Comparison of tensile properties of glass fibre reinforced polymer rebars by testing according to various standards," *Materials*, vol. 13, no. 18, Sep. 2020, doi: 10.3390/ma13184110.

[31] Y. J. You, J. H. J. Kim, S. J. Kim, and Y. H. Park, "Methods to enhance the guaranteed tensile strength of GFRP rebar to 900 MPa with general fiber volume fraction," *Constr. Build. Mater.*, vol. 75, pp. 54–62, Jan. 2015, doi: 10.1016/j.conbuildmat.2014.10.047.

[32] Y. Zhang, D. Gao, D. Fang, L. Yang, Y. Pang, and J. Tang, "Durability of graphene-modified epoxy vinyl resin served as matrix phase of composite bar in simulated concrete environment," *Journal of Building Engineering*, vol. 68, Jun. 2023, doi: 10.1016/j.jobe.2023.106106.

[33] "Test Method for Transverse Shear Strength of Fiber-reinforced Polymer Matrix Composite Bars," Mar. 01, 2011, *ASTM International, West Conshohocken, PA*. doi: 10.1520/D7617_D7617M-11.

[34] "Test Method for Transverse Shear Strength of Fiber-reinforced Polymer Matrix Composite Bars," Mar. 01, 2011, *ASTM International, West Conshohocken, PA*. doi: 10.1520/D7617_D7617M-11.

[35] M. Ahmad Sawpan, "Shear properties and durability of GFRP reinforcement bar aged in seawater," *Polym. Test.*, vol. 75, pp. 312–320, May 2019, doi: 10.1016/j.polymertesting.2019.02.033.

[36] D. Gao, Y. Zhang, F. Wen, Y. Pang, D. Fang, and M. Lv, "Transverse shear properties of fiber reinforced polymer bars with different reinforced phases," *J. Compos. Mater.*, vol. 55, no. 27, pp. 4063–4078, Nov. 2021, doi: 10.1177/00219983211031630.

[37] A. S. Genikomsou, G. P. Balomenos, P. Arczewska, and M. A. Polak, "Transverse Shear Testing of GFRP Bars with Reduced Cross Sections," *Journal of Composites for Construction*, vol. 22, no. 5, Oct. 2018, doi: 10.1061/(asce)cc.1943-5614.0000880.

[38] M. Ahmad Sawpan, "Shear properties and durability of GFRP reinforcement bar aged in seawater," *Polym. Test.*, vol. 75, pp. 312–320, May 2019, doi: 10.1016/j.polymertesting.2019.02.033.

[39] K. Ogrodowska and M. Urbański, "Nanosilica Modification of Epoxy Matrix in Hybrid Basalt-Carbon FRP Bars—Impact on Microstructure and Mechanical Properties," *Materials*, vol. 16, no. 5, Mar. 2023, doi: 10.3390/ma16051912.

[40] Y. Alaei, P. Cousin, M. Robert, and B. Benmokrane, "Effects of Graphene on the Moisture Absorption, Mechanical, Thermal, and Durability Properties of GFRP Bars," *Journal of Composites for Construction*, vol. 29, no. 6, Dec. 2025, doi: 10.1061/jccof2.cceng-5288.

[41] Y. Zhang, H. Cao, H. Zhu, J. Yuan, G. Chen, and D. Gao, "Shear performance of graphene nanosheet-modified ductile carbon/glass hybrid fiber-reinforced composite (C/G-HFRC) tendons along transverse direction," *Constr. Build. Mater.*, vol. 494, Oct. 2025, doi: 10.1016/j.conbuildmat.2025.143373.

[42] F. Yan, Z. Lin, and M. Yang, "Bond mechanism and bond strength of GFRP bars to concrete: A review," *Compos. B Eng.*, vol. 98, pp. 56–69, Aug. 2016, doi: 10.1016/j.compositesb.2016.04.068.

[43] G. M. Bueno and E. Bittencourt, "Study of Basalt Fibers and Graphene Enriched Polymers on Bond Behavior of FRP Bars in Concrete," *Applied Sciences (Switzerland)*, vol. 15, no. 11, Jun. 2025, doi: 10.3390/app15115838.

[44] B. M. R Ehsani, H. Saadatmanesh, and S. Tao, "DESIGN RECOMMENDATIONS FOR BOND OF GFRP REBARS TO CONCRETE."

[45] G. Fava, V. Carvelli, and M. A. Pisani, "Remarks on bond of GFRP rebars and concrete," *Compos. B Eng.*, vol. 93, pp. 210–220, May 2016, doi: 10.1016/j.compositesb.2016.03.012.

[46] M. Baena, L. Torres, A. Turon, and C. Barris, "Experimental study of bond behaviour between concrete and FRP bars using a pull-out test," *Compos. B Eng.*, vol. 40, no. 8, pp. 784–797, Dec. 2009, doi: 10.1016/j.compositesb.2009.07.003.

[47] Y. Ding, X. Ning, Y. Zhang, F. Pacheco-Torgal, and J. B. Aguiar, "Fibres for enhancing of the bond capacity between GFRP rebar and concrete," *Constr. Build. Mater.*, vol. 51, pp. 303–312, Jan. 2014, doi: 10.1016/j.conbuildmat.2013.10.089.

[48] R. Devaraj, A. Olofinjana, and C. Gerber, "On the Factors That Determine the Bond Behaviour of GFRP Bars to Concrete: An Experimental Investigation," *Buildings*, vol. 13, no. 11, Nov. 2023, doi: 10.3390/buildings13112896.

[49] S. Quayyum and B. S. Bangladesh, "BOND BEHAVIOUR OF FIBRE REINFORCED POLYMER (FRP) REBARS IN CONCRETE," 2010.

[50] D. Tong, Y. Chi, L. Huang, Y. Zeng, M. Yu, and L. Xu, "Bond performance and physically explicable mathematical model of helically wound GFRP bar embedded in UHPC," *Journal of Building Engineering*, vol. 69, Jun. 2023, doi: 10.1016/j.jobe.2023.106322.

[51] Y. Zhou *et al.*, "Experimental Investigations on Bond Behavior between FRP Bars and Advanced Sustainable Concrete," *Polymers (Basel).*, vol. 14, no. 6, Mar. 2022, doi: 10.3390/polym14061132.

[52] S. Soares, N. Freitas, E. Pereira, E. Nepomuceno, E. Pereira, and J. Sena-Cruz, "Assessment of GFRP bond behaviour for the design of sustainable reinforced seawater concrete structures," *Constr. Build. Mater.*, vol. 231, Jan. 2020, doi: 10.1016/j.conbuildmat.2019.117277.

[53] X. Hu, W. Xue, and W. Xue, "Bond properties of GFRP rebars in UHPC under different types of test," *Eng. Struct.*, vol. 314, Sep. 2024, doi: 10.1016/j.engstruct.2024.118319.

[54] M. Arabi and M. A. Noseir, "Bond Behaviour of FRP Bars Embedded in Concrete Elements.," 2024.

[55] J. J. Zeng *et al.*, "Bond behavior between concrete and thermoplastic GFRP bars with novel surface features," *Eng. Struct.*, vol. 343, Nov. 2025, doi: 10.1016/j.engstruct.2025.121161.

[56] X. Wang *et al.*, "Improving bond of fiber-reinforced polymer bars with concrete through incorporating nanomaterials," *Compos. B Eng.*, vol. 239, Jun. 2022, doi: 10.1016/j.compositesb.2022.109960.

[57] M. Al-Zu'bi, "From Neat Epoxy to Nanocomposites: Innovations in Bonding Systems for FRP-based Concrete Retrofitting: A Mini Review," *Engineering Science & Technology*, pp. 65–71, Nov. 2025, doi: 10.37256/est.7120268556.

[58] "Combar® glass-bre reinforcement." [Online]. Available: www.schoeck.com/conditions.

[59] J. Sena-Cruz, "Strengthening of Concrete Structures with Near-Surface Mounted CFRP Laminate Strips", PhD Thesis, University of Minho, (2005).

[60] L. Correia, A. Dushimimana, S. A. Jawed, J. M. Pereira, S. Cabral-Fonseca, and J. Sena-Cruz, "Durability of NSM CFRP-to-concrete bond after six years of exposure to laboratory and outdoor environments," *Constr. Build. Mater.*, vol. 537, Aug. 2026, doi: 10.1016/j.conbuildmat.2026.147100.